Journal of Computational Physics 228 (2009) 1116–1138

Contents lists available at ScienceDirect

Journal of Computational Physics

journal homepage: www.elsevier.com/locate/jcp

Gas-kinetic numerical studies of three-dimensional complex flows on spacecraft re-entry

Zhi-Hui Li [a,b,*], Han-Xin Zhang [a]

[a] National Laboratory for Computational Fluid Dynamics, No. 37 Xueyuan Road, Beijing 100191, China
[b] Hypervelocity Aerodynamics Institute, China Aerodynamics Research and Development Center, P.O. Box 211, Mianyang 621000, China

ARTICLE INFO

Article history:
Received 16 August 2007
Received in revised form 4 August 2008
Accepted 12 October 2008
Available online 18 October 2008

Keywords:
Kinetic theory of gases
Velocity distribution function
Boltzmann model equation
Discrete velocity ordinate method
Finite-difference computation
Three-dimensional complex flow
Spacecraft re-entry

ABSTRACT

The gas-kinetic numerical algorithm solving the Boltzmann model equation is extended and developed to study the three-dimensional hypersonic flows of spacecraft re-entry into the atmosphere in perfect gas. In this study, the simplified velocity distribution function equation for various flow regimes is presented on the basis of the kinetic Boltzmann–Shakhov model. The discrete velocity ordinate technique and numerical quadrature methods, such as the Gauss quadrature formulas with the weight function $2/\pi^{1/2}\exp(-V^2)$ and the Gauss–Legendre numerical quadrature rule, are studied to resolve the barrier in simulating complex flows from low Mach numbers to hypersonic problems. Specially, the gas-kinetic finite-difference scheme is constructed for the computation of three-dimensional flow problems, which directly captures the time evolution of the molecular velocity distribution function. The gas-kinetic boundary conditions and numerical procedures are studied and implemented by directly acting on the velocity distribution function. The HPF (high performance fortran) parallel implementation technique for the gas-kinetic numerical method is developed and applied to study the hypersonic flows around three-dimensional complex bodies. The main purpose of the current research is to provide a way to extend the gas-kinetic numerical algorithm to the flow computation of three-dimensional complex hypersonic problems with high Mach numbers. To verify the current method and simulate gas transport phenomena covering various flow regimes, the three-dimensional hypersonic flows around sphere and spacecraft shape with different Knudsen numbers and Mach numbers are studied by HPF parallel computing. Excellent results have been obtained for all examples computed.

© 2008 Elsevier Inc. All rights reserved.

1. Introduction

To study the aerodynamics of spacecraft re-entering Earth's atmosphere, Tsien [1] presented an interesting concept in terms of the degree of gas rarefaction: the gas flows can be approximately divided into four flow regimes based on the order of the Knudsen number (Kn), such as continuum flow, slip flow, transition flow, and free molecular flow. In fact, the aerothermodynamics around space vehicles are totally different in various flow regimes and take on the complex character of many scales. Especially, the gas flows in the near-continuum and rarefied transition regimes between the continuum regime and the free molecular regime have been difficult to treat either experimentally or theoretically. Actually, it has been a challenge how to effectively solve the complex problems covering various flow regimes. To simulate the gas flows from various regimes, the tra-

* Corresponding author. Address: National Laboratory for Computational Fluid Dynamics, No. 37 Xueyuan Road, Beijing 100191, China. Tel.: +86 10 8233 0957; fax: +86 10 8231 7341.
E-mail addresses: zhli0097@x263.net, lizhihui@mail.tsinghua.edu.cn (Z.-H. Li).

0021-9991/$ - see front matter © 2008 Elsevier Inc. All rights reserved.
doi:10.1016/j.jcp.2008.10.013

ditional way is to deal with them with different methods. On the one hand, the methods related to rarefied gas flow have been developed, such as the microscopic molecular-based direct simulation Monte-Carlo (DSMC) method [2]. On the other hand, also the methods adapted to continuum flow have been well developed, such as the solvers of macroscopic fluid dynamics in which the Euler, Navier–Stokes or Burnett-like equations are numerically solved. However, both methods are totally different in nature, and the computational results are difficult to link up smoothly with various flow regimes. Engineering development of current or intending spaceflight projects is closely concerned with complex gas dynamic problems of low-density flows in the intermediate range of Knudsen numbers [3–6], especially in the rarefied transition and in the near-continuum flow regimes.

The Boltzmann equation [7] can describe the molecular transport phenomena for the full spectrum of flow regimes and act as the main foundation for the study of complex gas dynamics. However, the difficulties encountered in solving the full Boltzmann equation are mainly associated with the nonlinear multidimensional integral nature of the collision term [7,8]. Moreover, up to these days, the exact solutions of the Boltzmann equation are almost impractical for the analysis of practical complex flow problems. Therefore, several methods for approximate solutions of the Boltzmann equation have been proposed to simulate only the simple flow [9–12]. It is still very difficult to solve it numerically due to binary collisions, of which in particular, the unknown character of the intermolecular counteractions. Furthermore, this leads to a very high cost with respect to velocity discretization and the computation of the five-dimensional collision integral.

From the kinetic-molecular theory of gases, numerous statistical or relaxation kinetic model equations resembling to the various order of moments of the original Boltzmann equation have been put forward [13–21]. The BGK equation, presented by Bhatnagar et al. [13], provides an effective and tractable way to deal with gas flows, which [13–15] supposes that the effect of collisions is roughly proportional to the departure of the true velocity distribution function from a Maxwellian equilibrium distribution. Subsequently, several kinds of nonlinear Boltzmann model equations have been developed: the ellipsoidal statistical (ES) model by Holway [16], Cercignani and Tironi [17], and Andries et al. [18], the generalization of the BGK model by Shakhov [19], the polynomial model by Segal and Ferziger [20], and the hierarchy kinetic model equation similar to the Shakhov model proposed by Abe and Oguchi [21]. Among the main features of these high-order generalizations of the BGK model, the Boltzmann model equations give the correct Prandtl number and possess the essential and average properties of the original and physical realistic equation. Once the distribution function can be solved, the macroscopic physical quantities of gas dynamics can be obtained by the moments of the distribution function multiplied by some functions of the molecular velocity over the entire velocity space. Thus, instead of solving the full Boltzmann equation, one solves the nonlinear kinetic model equations and probably finds a more economical and efficient numerical method for complex gas flows over a wide range of Knudsen numbers.

Based on the main idea from the kinetic theory of gases in which the Maxwellian velocity distribution function can be translated into the macroscopic physical variables of the gas flow in normal equilibrium state, some gas-kinetic numerical methods [22,23] have been developed to solve inviscid gas dynamics. Since the 1990s, applying the asymptotic expansion of the velocity distribution function to the standard Maxwellian distribution in terms of the flux conservation at the cell interface, the kinetic BGK-type schemes adapting to compressible continuum flow or near continuum flow [24–30] have been presented on the basis of the BGK model. Recently, the BGK scheme has also been extended [31–33] to study three-dimensional flow using general unstructured meshes. However, the computations of rarefied gas flows using the so-called kinetic models of the original Boltzmann equation have been advanced [34–39] commendably with the development of powerful computers and numerical methods since the 1960s. The high resolution explicit or implicit finite difference methods for solving the two-dimensional BGK–Boltzmann model equations have been set forth on the basis of the introduction of the reduced velocity distribution functions and the application of the discrete ordinate technique. In particular, the discrete-velocity model of the BGK equation which satisfies conservation laws and dissipation of entropy has been developed [40]. The reliability and efficiency of these methods have been demonstrated in applications to one- and two-dimensional rarefied gas dynamical problems in a monatomic gas. To describe the non-equilibrium flows in the transitional regime, the hybrid schemes coupling kinetic models of the Boltzmann equation with continuum solvers of the macroscopic fluid equations have been developed over the last decade [41–44] and applied to gas flows of high altitude flights and micro systems.

In this work, we are essentially dealing with developing the gas-kinetic numerical algorithm for the direct solution of the Boltzmann kinetic relaxation model, in which the Boltzmann model equation can be translated into hyperbolic conservation systems with nonlinear source terms in physical space and time by first developing the discrete ordinate method in the gas kinetic theory. Then the gas-kinetic numerical schemes are constructed by using the time-splitting method for unsteady equation and the finite difference technique in computational fluid dynamics. In two earlier papers [45,46], the gas-kinetic numerical method has been successively presented and applied to simple supersonic gas flows with low Mach numbers. In this paper, the gas-kinetic algorithm will be extended and developed to investigate three-dimensional complex flow problems covering various flow regimes, particularly in the rarefied transition and near-continuum flow regimes, for possible engineering applications. The uniqueness of the present paper consists in using the Boltzmann simplified velocity distribution function equation for simulations of the three-dimensional complex problems from rarefied to continuum regimes with high Mach numbers. This is the first attempt to study and use the direct Boltzmann gas-kinetic solver to compute the three-dimensional hypersonic flows covering various flow regimes with a wide range of Mach numbers. The new discrete velocity ordinate technique and numerical quadrature methods, gas-kinetic boundary conditions and numerical procedures, and the gas-kinetic numerical scheme for three-dimensional complex flows with parallelization are developed directly to capture the time evolution of the velocity distribution function. At the beginning of the gas-kinetic numerical studies in three-dimensional complex hypersonic flows, the fluid medium is taken as the perfect gas without consideration of the internal, energy

relaxation and the effects of rotational and vibrational temperature in this paper. The remaining part of the paper is organized as follows. In Section 2, the gas-kinetic numerical algorithm explicitly solving the velocity distribution function will be presented for three-dimensional complex flows, and then, respectively the discrete velocity numerical quadrature methods for high Mach number flows and the gas-kinetic boundary conditions for the velocity distribution function will be studied. In Section 3, the HPF parallel implementation and efficiency of the gas-kinetic algorithm will be investigated. In Section 4, numerous numerical results for the three-dimensional complex flows and gas transfer phenomena covering various flow regimes will be presented to demonstrate the feasibility and to validate the accuracy of the numerical methods. Finally, some concluding remarks will be given in Section 5.

2. Gas-kinetic numerical algorithm for three-dimensional complex flows

2.1. Gas-kinetic numerical scheme of direct solving the velocity distribution function

The Boltzmann equation describes the time evolution of the statistical distribution function in the position space $\vec{r} = (x, y, z)$ and velocity space $\vec{V} = (V_x, V_y, V_z)$ by the mathematical model of the non-equilibrium kinetic theory of gases, which represents the relationships between the molecular velocity distribution function that provides a statistical description of a gas and the variables on which it depends. A large amount of the detail of the two-body interaction, which is contained in the Boltzmann collision operator, is unlikely to influence significantly the values of the macroscopic quantities [7,8,47]. It is, therefore, enlightened that the Boltzmann collision integral can be replaced by a simplified collision operator which retains the essential and non-equilibrium kinetic properties of the actual collision operator. Then, however, any replacement of the collision function must satisfy the conservation of mass, momentum and energy expressed by the Boltzmann equation. We consider a class of Boltzmann model equations of the form

$$\frac{\partial f}{\partial t} + \vec{V} \cdot \frac{\partial f}{\partial \vec{r}} = \nu(f^N - f), \tag{1}$$

where $f(\vec{r}, \vec{V}, t)$ is the molecular velocity distribution function which depends on space $\vec{r}$, molecular velocity $\vec{V}$ and time t. The collision frequency ν and the local equilibrium distribution function f^N can be integrated with the macroscopic flow parameters, the molecular viscosity transport coefficient, the thermodynamic effect, the molecular power law models, and the flow state controlling parameter from various flow regimes [46,48]. The ν of the gas molecules can be extended and expressed as the function of density, temperature, the free-stream mean free path, and the exponent of molecular power law

$$\nu = \frac{16}{5}\sqrt{\frac{R}{2\pi}} \cdot \frac{T_\infty^{\chi-1/2}}{n_\infty} \cdot \frac{1}{\lambda_\infty} \cdot \frac{n}{T^{\chi-1}}. \tag{2}$$

The f^N is taken as the asymptotic expansion in Hermite polynomials with the local Maxwell distribution function f_M as the weighting function [19,35]:

$$f^N = f_M \cdot [1 + (1 - \Pr)\,\vec{c} \cdot \vec{q}(c^2/(RT) - 5)/(5PRT)], \tag{3}$$

$$f_M = \frac{n}{(2\pi RT)^{3/2}} \exp\left(-\frac{c^2}{2RT}\right). \tag{4}$$

Here, Pr is the Prandtl number as the ratio of the coefficient of viscosity μ and heat conduction K with $Pr = \mu C_p/K$, C_p is the specific heat at constant pressure, and $\vec{q}$ and P, respectively denote the heat flux vector and gas pressure.

Actually for non-homogeneous gas flow, the interaction of gas viscosity is produced from the transfer of molecular momentum between two contiguous layers of the mass flow due to the motion of molecules. However, when the gas mass interchanges between the two layers with different temperature, the transfer of heat energy results in the thermodynamic effect. The thermodynamic effect of the real gas flow is reflected in Eq. (3) of the f^N by using the Prandtl number to relate the coefficient of viscosity with heat conduction from the molecular transport of gas. All of the macroscopic flow variables of gas dynamics in consideration, such as the density of the gas ρ, the flow velocity $\vec{U}$, the temperature T, the pressure P, the viscous stress tensor τ and the heat flux vector $\vec{q}$, can be evaluated by the following moments of the velocity distribution function over the velocity space.

$$n(\vec{r}, t) = \int f(\vec{r}, \vec{V}, t)\, d\vec{V}, \quad \rho(\vec{r}, t) = mn(\vec{r}, t), \tag{5}$$

$$n\vec{U}(\vec{r}, t) = \int \vec{V} f(\vec{r}, \vec{V}, t)\, d\vec{V}, \tag{6}$$

$$\frac{3}{2} nRT(\vec{r}, t) = \int \frac{1}{2} c^2 f(\vec{r}, \vec{V}, t)\, d\vec{V}, \tag{7}$$

$$P(\vec{r}, t) = n(\vec{r}, t) kT(\vec{r}, t), \tag{8}$$

$$\tau_{ij}(\vec{r}, t) = m \int c_i c_j f(\vec{r}, \vec{V}, t)\, d\vec{V} - P\delta_{ij}, \tag{9}$$

$$\vec{q}(\vec{r}, t) = m \int \frac{1}{2} c^2\, \vec{c}\, f(\vec{r}, \vec{V}, t)\, d\vec{V}, \tag{10}$$

where m denotes the molecular mass, R is the gas constant, k is the Boltzmann's constant, and the subscripts i and j each range from 1 to 3, where the values 1, 2, and 3 may be identified with components along the x-, y-, and z-directions, respectively.

Since the formulated problem involves in the scale of the microscopic statistical distribution and the macroscale of gas flow with tremendous difference of dimension order, the non-dimensionalized procedure of variables and equations is needed to unify the scale in practical computation. Generally, four independent reference variables should be set in the non-dimensional reference system of the computation of gas flows. In here, let L_{ref}, T_∞, n_∞, and m be, respectively, the reference length, the free-stream temperature, the free-stream number density, and molecular mass, and put the reference speed and time as $c_{m\infty} = \sqrt{2RT_\infty}$ and $t_\infty = L_{ref}/c_{m\infty}$. Then, the non-dimensional variables are defined as time $\tilde{t} = t/t_\infty$, flow velocity $\tilde{U}_i = U_i/c_{m\infty}$, molecular velocity $\tilde{V}_i = V_i/c_{m\infty}$, $(i = 1,2,3)$, number density of gas flow $\tilde{n} = n/n_\infty$, temperature $\tilde{T} = T/T_\infty$, pressure $\tilde{p} = p/(mn_\infty c_{m\infty}^2/2)$, stress tensor $\tilde{\tau}_{ij} = \tau_{ij}/(mn_\infty c_{m\infty}^2/2)$, heat flux vector $\tilde{q}_i = q_i/(mn_\infty c_{m\infty}^3/2)$, space position $\tilde{x} = x/L_{ref}$, $\tilde{y} = y/L_{ref}$, $\tilde{z} = z/L_{ref}$, collision frequency $\tilde{\nu} = \nu \cdot t_\infty$, velocity distribution function $\tilde{f} = f/(n_\infty/c_{m\infty}^3)$, Maxwellian distribution $\tilde{f}_M = f_M/(n_\infty/c_{m\infty}^3)$, and local equilibrium distribution $\tilde{f}^N = f^N/(n_\infty/c_{m\infty}^3)$. The dimensionless velocity distribution function equation can be obtained by non-dimensionalizing Eqs. (1)–(4) with the above non-dimensional variables

$$\frac{\partial \tilde{f}}{\partial \tilde{t}} + \tilde{\vec{V}} \cdot \frac{\partial \tilde{f}}{\partial \tilde{\vec{r}}} = \tilde{\nu}(\tilde{f}^N - \tilde{f}), \tag{11}$$

$$\tilde{f}^N = \tilde{f}_M \cdot [1 + (1 - \mathrm{Pr})\tilde{\vec{c}} \cdot \tilde{\vec{q}}(2\tilde{c}^2/\tilde{T} - 5)/(5\tilde{P}\tilde{T}/2)], \tag{12}$$

$$\tilde{f}_M = \frac{\tilde{n}}{(\pi\tilde{T})^{3/2}} \exp(-\tilde{c}^2/\tilde{T}), \tag{13}$$

$$\tilde{\nu} = \frac{8\tilde{n}\tilde{T}^{1-\chi}}{5\sqrt{\pi}Kn}, \quad Kn = \frac{\lambda_\infty}{L_{ref}}, \tag{14}$$

where Kn is the Knudsen number as an important parameter characterizing the degree of rarefaction of the gas, λ_∞ is the free-stream mean free path, and $\tilde{\vec{c}}$ represents the thermal velocity of the molecule, that is $\tilde{\vec{c}} = \tilde{\vec{V}} - \tilde{\vec{U}}$.

Similarly, the non-dimensional macroscopic variables can be represented by non-dimensionalizing Eqs. (5)–(10). In the following computation, all of the variables will have been non-dimensionalized, and the "$\sim$" sign in the equations will be dropped for the simplicity and concision without causing any confusion.

Eq. (11) provides the statistical description of the gas flow in any non-equilibrium state from the level of the kinetic theory of gases. Since mass, momentum and energy are conserved during molecular collisions, Eq. (11) satisfies the Boltzmann's H-theorem and conservation conditions at each of points in physical space and time

$$\int (f^N - f)\psi^{(m)} d\vec{V} = 0, \tag{15}$$

where $\psi^{(m)}$ are the components of the moments on mass, momentum and energy, that is

$$\psi^{(1)} = 1, \quad \psi^{(2)} = \vec{V}, \quad \psi^{(3)} = |\vec{V}|^2/2. \tag{16}$$

The focus under consideration is how the velocity distribution function can be numerically solved. The distribution function f is a probability density function of statistical distribution [8,47]. In order to replace the continuous dependency of f on the velocity space, the discrete ordinate method can be introduced and developed [37,45,46,49] from point of view of the gas kinetic theory. The discrete ordinate technique consists of replacing the integration over the velocity space of the distribution function by an appropriate quadrature. This requires approximating the velocity dependence of the distribution function by a set of functions, each evaluated at appropriate discrete points in velocity space. The discrete velocity ordinate (DVO) method and quadrature formula presented in [46] are fit for low Mach number flows. To simulate the three-dimensional hypersonic flows, the specific DVO technique and numerical quadrature are developed and described in Section 2.3. Applying the DVO method to Eq. (11) for the (V_x, V_y, V_z) velocity space, the single velocity distribution function equation can be transformed into hyperbolic conservation equations with nonlinear source terms at each of DVO points $(V_{x\sigma}, V_{y\delta}, V_{z\theta})$, which can be written in the transformed coordinates (ξ, η, ζ), as follows:

$$\frac{\partial U}{\partial t} + \frac{\partial F}{\partial \xi} + \frac{\partial G}{\partial \eta} + \frac{\partial H}{\partial \zeta} = S, \tag{17}$$

with

$$U = JQ, \quad F = \overline{U}U, \quad G = \overline{V}U,$$
$$H = \overline{W}U, \quad S = J\overline{S},$$

where

$$\overline{U} = V_{x\sigma}\xi_x + V_{y\delta}\xi_y + V_{z\theta}\xi_z, \quad \overline{V} = V_{x\sigma}\eta_x + V_{y\delta}\eta_y + V_{z\theta}\eta_z, \quad \overline{W} = V_{x\sigma}\zeta_x + V_{y\delta}\zeta_y + V_{z\theta}\zeta_z,$$
$$J = \partial(x,y,z)/\partial(\xi,\eta,\zeta), \quad Q = f_{\sigma,\delta,\theta}, \quad \overline{S} = \nu(f^N_{\sigma,\delta,\theta} - f_{\sigma,\delta,\theta}).$$

To solve the governing Eq. (17) at each of $(V_{x\sigma}, V_{y\delta}, V_{z\theta})$ for three-dimensional flow, the time-splitting numerical method can be adopted in the light of the unsteady characteristic of molecular convective movement and colliding relaxation, and the value of U in Eq. (17) at time $n+1$ can be expressed by second-order Taylor series expansion:

$$U^{n+1} = \left[1 - \overline{U}\Delta t\delta_{\xi} + \frac{\overline{U}^2}{2}\Delta t^2\delta_{\xi^2}\right]\cdot\left[1 - \overline{V}\Delta t\delta_{\eta} + \frac{\overline{V}^2}{2}\Delta t^2\delta_{\eta^2}\right]\cdot\left[1 - \overline{W}\Delta t\delta_{\zeta} + \frac{\overline{W}^2}{2}\Delta t^2\delta_{\zeta^2}\right]\cdot\left[1 - v\Delta t\left(1 - \frac{v}{2}\Delta t\right)\right]U^n + O(\Delta t^2, \Delta\xi^2, \Delta\eta^2, \Delta\zeta^2). \tag{18}$$

The above finite difference approximation can be split as the following four operators:

$$U^* = L_S(\Delta t)U^n = U^n + \left(1 - \frac{v}{2}\Delta t\right)\Delta t\cdot S^n, \tag{19}$$

$$U^{**} = L_{\zeta}(\Delta t)U^* = \left[1 - \overline{W}\Delta t\delta_{\zeta} + \frac{\overline{W}^2\Delta t^2}{2}\delta_{\zeta^2}\right]U^*, \tag{20}$$

$$U^{***} = L_{\eta}(\Delta t)U^{**} = \left[1 - \overline{V}\Delta t\delta_{\eta} + \frac{\overline{V}^2\Delta t^2}{2}\delta_{\eta^2}\right]U^{**}, \tag{21}$$

$$U^{n+1} = L_{\xi}(\Delta t)U^{***} = \left[1 - \overline{U}\Delta t\delta_{\xi} + \frac{\overline{U}^2\Delta t^2}{2}\delta_{\xi^2}\right]U^{***}. \tag{22}$$

In fact, the finite difference Eqs. (19)–(22) are respectively consistent with four differential equations in the following:

$$\frac{\partial U}{\partial t} = S, \tag{23}$$

$$\frac{\partial U}{\partial t} + \frac{\partial H}{\partial \zeta} = 0, \tag{24}$$

$$\frac{\partial U}{\partial t} + \frac{\partial G}{\partial \eta} = 0, \tag{25}$$

$$\frac{\partial U}{\partial t} + \frac{\partial F}{\partial \xi} = 0. \tag{26}$$

According to the time-splitting method, on each time interval Δt, a solution of Eq. (17) is substituted by a solution of a sequence of four Eqs. (23)–(26). Then, the colliding relaxation Eq. (23) can be numerically integrated by using the second-order Runge–Kutta method:

$$\begin{aligned}
&\delta_t U^* = \left(1 - \frac{v}{2}\Delta t\right)\cdot S(U^n),\\
&U^* = U^n + \Delta t\cdot\delta_t U^*,\\
&\delta_t U^{**} = \left(1 - \frac{v}{2}\Delta t\right)\cdot S(U^*),\\
&U^{n+1} = U^n + \frac{\Delta t}{2}(\delta_t U^* + \delta_t U^{**}).
\end{aligned} \tag{27}$$

The convective movement Eqs. (24)–(26) in the (ζ, η, ξ) directions of the position space can be numerically solved by using the NND-4(a) finite-difference scheme [50] based on primitive variables, which is a two-stage scheme with second-order accuracy in time and space. For Eq. (24), the finite-difference scheme can be expressed as

$$U^* = U^n - \frac{\Delta t}{\Delta\zeta}(Q^n_{i+1/2} - Q^n_{i-1/2}), \tag{28}$$

$$U^{n+1} = \frac{1}{2}\left[U^n + U^* - \frac{\Delta t}{\Delta\zeta}(Q^*_{i+1/2} - Q^*_{i-1/2})\right], \tag{29}$$

$$\begin{aligned}
&Q_{i+1/2} = H^+_{i+1/2}(U_L) + H^-_{i+1/2}(U_R),\\
&U_{L,i+1/2} = U_{p,i} + \frac{1}{2}\min\mathrm{mod}(\Delta U_{p,i-1/2}, \Delta U_{p,i+1/2}),\\
&U_{R,i+1/2} = U_{p,i+1} - \frac{1}{2}\min\mathrm{mod}(\Delta U_{p,i+1/2}, \Delta U_{p,i+3/2}),\\
&\Delta U_{p,i+1/2} = U_{p,i+1} - U_{p,i},
\end{aligned}$$

where U_p denotes the primitive variable of Eq. (24), and $H^{\pm}$, respectively denote the flux vector splitters of H based on the positive and negative characteristic values $\lambda^{\pm}$ with $\lambda^+ = (\lambda + |\lambda|)/2$ and $\lambda^- = (\lambda - |\lambda|)/2$. The flux limiter min mod operator in the above-mentioned scheme is defined by

$$\min\mathrm{mod}(x, y) = \frac{1}{2}[\mathrm{sgn}(x) + \mathrm{sgn}(y)]\cdot\min(|x|, |y|). \tag{30}$$

Considering simultaneously proceeding on the molecular movement and colliding relaxation in real gas, the computing order of the previous and subsequent time steps is interchanged to couple to solve them in the computation. The second-order finite difference scheme directly solving the six-dimensional discrete velocity distribution functions is set as

$$U^{n+1} = L_S\left(\frac{\Delta t}{2}\right)L_\zeta\left(\frac{\Delta t}{2}\right)L_\eta\left(\frac{\Delta t}{2}\right)L_\xi(\Delta t)L_\eta\left(\frac{\Delta t}{2}\right)L_\zeta\left(\frac{\Delta t}{2}\right)L_S\left(\frac{\Delta t}{2}\right)U^n. \tag{31}$$

In view of the behaviour of the time evolution on the velocity distribution function and the decoupling technique [2,5,51] on molecular motion and intermolecular collisions in the DSMC method, the time step size (Δt) in the computation should be controlled by coupling the stability condition (Δt_s) of the scheme with the local mean collision time interval (Δt_c), thus we have

$$\Delta t = \min(\Delta t_s, \Delta t_c), \tag{32}$$

with

$$\Delta t_s = \frac{CFL}{\max\left(\frac{v}{2}, \frac{|\bar{U}|}{\Delta\xi}, \frac{|\bar{V}|}{\Delta\eta}, \frac{|\bar{W}|}{\Delta\zeta}\right)}, \Delta t_c = \frac{1}{v_{\max}},$$

where *CFL* is the adjusting coefficient of the time step in the scheme, that can be set as *CFL* = 0.99.

For constructing an effective numerical scheme (31) in solving three-dimensional complex flows, the finite difference scheme which approximates the velocity distribution function Eq. (17) must possess the properties of monotonicity and conservation. The conservative finite-difference schemes are constructed for each separate step in Eqs. (23)–(26), and then the whole scheme is conservative. In the computation of the velocity distribution function, to guarantee the positivity of the distribution function for different Mach number flows, only those DVO points are considered, at which the distribution function is greater than a prescribed lower threshold. If at each iteration the time step is fixed according to the condition (32), the scheme (31) is perfectly conservative for mass, momentum, and total energy, and the positivity of the distribution function can be preserved.

2.2. Gas-kinetic boundary conditions and numerical procedures for the velocity distribution function

Since the present gas-kinetic algorithm explicitly evaluates the time evolution of the molecular velocity distribution function at each of discrete grid points from the physical space and velocity space, all kinds of boundaries should be numerically implemented by directly acting on the velocity distribution function instead of using the macroscopic flow variables. The hyperbolic type of the convective part of the Boltzmann model equation controls and determines the appropriate values of the distribution function in the boundaries. The boundaries can be divided into two parts of Γ_b and Γ_w, respectively corresponding to the boundary of the external free flow and to the surface of a body.

2.2.1. Gas-surface boundary

Thanks to the interaction of the gas molecules with the solid walls, one can trace the origin of the aerodynamics exerted by the gas upon the body and the heat transfer between the gas and the solid boundary Γ_w. The interaction depends on the surface finish, the cleanliness of the surface and its temperature [52]. In general, the interaction of a given molecule with the surface may also depend on the velocity distribution function of molecules impinging on a surface element. Hence, it is more convenient to think in terms of a probability density $R(\vec{V} \to \vec{V}'; \vec{r})$ [47] that a molecule hitting the solid boundary at some point $\vec{r}$ with some velocity $\vec{V}$ reemerges practically at the same point with some other velocity $\vec{V}'$. If R is known, then the boundary conditions for the molecular velocity distribution function $f(\vec{r}, \vec{V}, t)$ can be easily written down. The general form of the boundary conditions can be written by the aid of the surface balance condition of the mass flux (number of molecules leaving or arriving per unit time and unit area) as

$$|\vec{c}' \cdot \vec{n}| f(\vec{r}, \vec{V}', t) = \int_{\vec{c}\cdot\vec{n}<0} R(\vec{V} \to \vec{V}'; \vec{r}) f(\vec{r}, \vec{V}, t) |\vec{c} \cdot \vec{n}| d\vec{V}, \quad (\vec{r} \in S, \vec{c}' \cdot \vec{n} > 0). \tag{33}$$

In view of the difficulty of computing the scattering kernel $R(\vec{V} \to \vec{V}'; \vec{r})$ due to the complex physical phenomena of adsorption and evaporation which take place at the wall, mathematical models [47,52–54], that satisfy the basic physical requirements of normalization, positivity and preservation of local equilibrium at the wall, have been proposed. In particular, the scattering kernel corresponding to the Maxwell-type model is used in this paper. By defining the accommodation coefficient which describes how much the molecules accommodate to the state of the wall, the scattering kernel turns out to be

$$R(\vec{V} \to \vec{V}'; \vec{r}) = \alpha f_M^w(\vec{V}', \vec{r}) |\vec{c}' \cdot \vec{n}| + (1-\alpha)\delta(\vec{V}' - \vec{V} + 2\vec{n}(\vec{c} \cdot \vec{n})), \quad (\vec{c}' \cdot \vec{n} > 0, \vec{c} \cdot \vec{n} < 0). \tag{34}$$

According to this model for the scattering kernel, a fraction $(1-\alpha)$ of molecules undergoes a specular reflection, while the remaining fraction α is diffused with the Maxwellian distribution f_M^w of the wall. In general, α turns out to depend on the distribution function of the impinging molecules. A complete accommodation is when the molecules are conserved in number, but otherwise forget completely their impinging distribution. The emerging distribution is then proportional to f_M^w with temperature and mass velocity equal to the temperature and mass velocity of the wall, this gas is in thermal and mechanical

equilibrium with the wall. The opposite case with $\alpha = 0$ is when the gas remembers as much as possible of the impinging distribution, then the kernel is a delta function, and all the accommodation coefficients vanish so that the specular reflection is gained

$$R(\vec{V} \to \vec{V}'; \vec{r}) = \delta(\vec{V}' - \vec{V} + 2\vec{n}(\vec{c} \cdot \vec{n})). \tag{35}$$

In this case, the gas molecules are specularly reflected with the normal component of velocity reversed, therefore the gas cannot exert any stress on the surface, except in the direction of the normal. In fact, if the boundary conditions do not contain the temperature of the wall with the case of a completely reflected gas, then they would allow the gas to stay in thermal equilibrium at any given temperature, irrespective of the surrounding bodies. It is clear that these boundary conditions are quite unrealistic.

In general, the Maxwell-type boundary conditions give satisfactory results with values of α rather close to 1, and in problems where the gas dynamics and momentum transfer are primarily reckoned for the perfect gas without regarding to internal energy transfer, $\alpha = 1$ is a rather accurate assumption. For practical applications, Maxwell's boundary conditions with $\alpha = 1$ are frequently used for the simplicity and reasonable accuracy, and they are a reasonable approximation to any kind of more complicated boundary conditions [53–55]. In all the calculations in this paper, the aforementioned model of gas-surface interaction is implemented and used. According to the condition of the stationary solid wall that no particles penetrate the wall, all molecules striking the solid surface at any time must be reflected back to the gas. If the molecules strike on the surface, the molecular velocity distribution function, which is reflected from the surface, is considered as the form of "drifting Maxwellian" fully accommodating to the wall temperature T_w and velocity (U_w, V_w, W_w), which is set in discretized form as follows:

$$f_{\Gamma_w \sigma,\delta,\theta} = \frac{n_w}{(\pi T_w)^{3/2}} \exp\left[-\frac{(V_{x\sigma} - U_w)^2 + (V_{y\delta} - V_w)^2 + (V_{z\theta} - W_w)^2}{T_w}\right], \quad \vec{c} \cdot \vec{n} \geqslant 0, \tag{36}$$

where $\vec{n}$ is the unit vector normal to the wall surface, pointing to the gas.

The number density of molecules diffusing from the solid surface, n_w, which is not known previously and varied with the velocity distribution of incident molecules and the appearance of the solid surface, can be derived from the insulated condition of zero mass flux [12,36,48] normal to the wall surface

$$\int_{c_n>0} c_n f_M^w d\vec{V} = \int_{c_n<0} -c_n f d\vec{V}. \tag{37}$$

Then, substituting the Maxwellian distribution, characterized by the surface temperature T_w, into the left side of Eq. (37), one has

$$\frac{n_w}{(\pi T_w)^{3/2}} \iiint_{c_n>0} c_n \cdot e^{-\frac{V_x^2+V_y^2+V_z^2}{T_w}} dV_x dV_y dV_z = \iiint_{c_n<0} -c_n \cdot f dV_x dV_y dV_z. \tag{38}$$

As a consequence, the n_w in the preceding reflected distribution function can be obtained

$$n_w = -2\left(\frac{\pi}{T_w}\right)^{1/2} \iiint_{c_n<0} c_n^- \cdot f dV_x dV_y dV_z, \tag{39}$$

where $c_n^- = (c_n - |c_n|)/2$.

If $\vec{c} \cdot \vec{n} < 0$, the discrete velocity distribution functions at the wall grid points of the boundary Γ_w are solved by using second-order upwind-difference approximations from the adjacent grids in the interior of the flow field.

2.3. Outer boundary

The distribution function is assumed to be in equilibrium at infinity. However, the outer boundary Γ_b must be in some finite distance from the body, so the outer boundary conditions are numerically treated using characteristic-based boundary conditions. These are in accord with the upwind nature of the interior point scheme. From this standpoint, the distribution functions for outgoing molecules through the outer boundary are numerically solved by the second-order finite difference approximation from the interior points, where $\overline{W} > 0$.

For molecules incoming from outside, the characterizing condition $\overline{W} \leqslant 0$ is satisfied for the outer boundary, and the following approximation conditions are used.

(1) One can suppose that the condition $\vec{V}_\infty \cdot \vec{n}_b < 0$ is valid along the upstream boundary, where $\vec{n}_b$ is the outward vector normal to the outer boundary and $\vec{V}_\infty$ is the undisturbed free stream velocity, a function describing the undisturbed outer flow is accepted for the part Γ_{b1} of the outer boundary Γ_b ahead of the body, and the distribution functions of the ingoing molecules are set as the local equilibrium distribution with prescribed free stream properties. As a rule, the equilibrium distribution function for the molecules directed into the domain of the flow field is imposed for points of the free boundary surface Γ_{b1} in discretized form as follows:

$$f_{\Gamma_{b1}\sigma,\delta,\theta} = f_{M\sigma,\delta,\theta} \cdot \left[1 + (1 - \mathrm{Pr})\vec{c}_{\sigma,\delta,\theta} \cdot \vec{q}(2c^2_{\sigma,\delta,\theta}/T - 5)/(5PT/2)\right], \tag{40}$$

$$f_{M\sigma,\delta,\theta} = n/(\pi T)^{3/2} \exp[-c^2_{\sigma,\delta,\theta}/T], \tag{41}$$

where n, T, P, $\vec{U}$ are density, temperature, pressure and the vector of mean velocity of undisturbed gas flow.

(2) For the other part Γ_{b2} of the free boundary surface Γ_b, where $\vec{V}_\infty \cdot \vec{n}_b \geqslant 0$ in the downstream boundary, it is assumed that there is no gradient along the outward ς-direction for the distribution functions, which is, for incoming molecules

$$\frac{\partial \Delta U}{\partial \zeta} = 0 \quad \text{for} \quad \overline{W} \leqslant 0, \quad \vec{V}_\infty \cdot \vec{n}_b \geqslant 0. \tag{42}$$

2.4. Development of numerical integration methods for evaluating macroscopic flow moments

Once the discrete velocity distribution functions $f_{\sigma,\delta,\theta}$ are solved, the macroscopic flow moments at any time in each point of the physical space can be evaluated and updated by the appropriate discrete velocity quadrature method. The choice of the discrete velocity points and the quadrature scheme in the DVO method is somewhat determined by the problem dependent. In the general case, it is a complex problem to construct a system of points in the velocity space so that all particle velocities after collisions also belong to this system, which are similar to the velocity discretization of the Gaussian integration method from Refs. [56–58]. The size of the discrete velocity domain as a rule should be ensured in such a way that the contribution from the integration of the velocity distribution function over the complement of this domain is negligible. The appropriate discrete velocity numerical quadrature and the computational domain in the DVO method should be selected for more accuracy by one order than the required precision of the global computation. In this study, the specific Gauss-type integration methods, such as the Gauss quadrature formulas with the weight function $2/\pi^{1/2}\exp(-V^2)$ and the Gauss–Legendre numerical quadrature rule whose integral nodes are determined by using the roots of the kth-order Legendre polynomials, will be presented and applied to simulate hypersonic flows with a wide range of Mach numbers.

The basic idea of the Gauss-type quadrature method [59] is to choose the fixed evaluation points V_σ and the corresponding weight coefficients W_σ of the integration rule in a way that the following approximation is exact

$$\int_D W(V) f(V) dV \approx \sum_{\sigma=1}^{N} W_\sigma f(V_\sigma). \tag{43}$$

If both limits of the integration are infinite, a weighting function must be chosen that goes to zero for both positive and negative values of V. In the kinetic theory of rarefied gases, this choice of weight function leads naturally to a family of orthonormal basis functions defined by the products of a Maxwellian with the conventional Hermite polynomials. The Hermite polynomials are used to define the Gaussian quadrature rule for the velocity distribution function in equilibrium state [56–58], in which the Hermite weight function on the entire real line is used with the symmetric collocation points about zero in the velocity space. However, the Maxwellian distribution is an ideal equilibrium solution of the Boltzmann equation in the limit of continuum flow. Thus, the velocity distribution of high speed flow commonly deviates from the standard Maxwellian distribution, and takes on the unsymmetrical property in the real line of the velocity space. To develop the Gaussian integration method for the supersonic flows, the bell-shaped Gauss-type distribution function is introduced

$$W(V) = \frac{2}{\pi^{1/2}} \exp(-V^2), \quad -\infty < V < \infty. \tag{44}$$

When this weighting function (44) is used over the interval $[0,\infty)$, according to Eq. (43), the resulting Gauss quadrature formula with the weight function $2/\pi^{1/2}\exp(-V^2)$ is referred to as

$$\int_0^\infty \frac{2}{\pi^{1/2}} \exp(-V^2) f(V) dV \approx \sum_{\sigma=1}^{N} W_\sigma f(V_\sigma), \tag{45}$$

where V_σ ($\sigma = 1,\ldots,N$) are the positive roots of the orthogonal polynomials, $p_\sigma(V)$, in which the polynomials are generated by the following recurrence relation

$$p_\sigma(V) = (V - b_\sigma) p_{\sigma-1}(V) - g_\sigma p_{\sigma-2}(V), \tag{46}$$

with $p_0(V) = 1$ and $p_{-1}(V) = 0$. Here, b_σ and g_σ are the recurrence relation parameters [60] for the orthogonal polynomials associated with $\exp(-V^2)$ on $[0,\infty)$.

The nodes V_σ and weights W_σ of the Gauss quadrature rule (45) can be calculated from the recurrence relation by applying the QR algorithm [61] to determine the eigenvalues and the first component of the orthonormal eigenvectors of the associated $N \times N$ tridiagonal matrix eigensystem. The Gaussian quadrature will exactly integrate a polynomial of a given degree with the least number of quadrature points and weights. In particular, M-point Gaussian quadrature exactly integrates a polynomial of degree $2M - 1$. Therefore, the use of the Gaussian quadrature points and weights would seem to be the optimum choice to the considered integration in the sense.

Since the discrete velocity solution can be treated in terms of expansion on the basis of piecewise constant functions, the computation of the moments of the distribution function can be performed by the network in the discretized velocity space. For example, the gas density is evaluated by the Gauss quadrature formula with the weight function $2/\pi^{1/2}\exp(-V^2)$ in the following manner:

$$n = \int_{-\infty}^{\infty}\int_{-\infty}^{\infty}\int_{-\infty}^{\infty} f dV_x dV_y dV_z \approx \frac{\pi^{3/2}}{8}\sum_{\theta=-N_3}^{N_3}\sum_{\delta=-N_2}^{N_2}\sum_{\sigma=-N_1}^{N_1} W_\theta W_\delta W_\sigma f_{\sigma,\delta,\theta} e^{V_{x\sigma}^2} e^{V_{y\delta}^2} e^{V_{z\theta}^2}. \tag{47}$$

The other macroscopic flow moments, such as mean velocity, temperature, stress tensor and heat flux vector components, can be similarly evaluated according to the Gauss-type quadrature formula (45).

As the aforementioned Gauss-type quadrature rule with the weight function $2/\pi^{1/2}\exp(-V^2)$ merely employs some finite evaluation points to integrate the flow moments over the whole of velocity space, in practical application, it is quite efficacious to evaluate the macroscopic flow variables with high precision, in particular for intermediate Mach number flows. However, for hypersonic flows with high Mach numbers, the velocity distribution severely deviates from the Maxwellian equilibrium with a long trail of the unsymmetrical bimodal distribution in the real line of the velocity space, so that the extensive region of the velocity space depended on distribution function need to be discretized in quite a wide range, the number of DVO points needed to cover the appropriate velocity range becomes quite large, and then the composite Gauss–Legendre quadrature rule is developed and applied to this study. The Gauss–Legendre quadrature formula for evaluation of definite integrals with the interval $[-1,1]$ can be written as

$$\int_{-1}^{1} f(t)dt \approx \sum_{i=1}^{n} A_i f(t_i), \tag{48}$$

where t_i is the evaluation point taken as the roots of a special family of polynomials called the Legendre polynomials, in which the first two Legendre polynomials are $p_0(t) = 1$ and $p_1(t) = t$, and the remaining members of the sequence are generated by the following recurrence relation

$$(n+1)p_{n+1}(t) = (2n+1)tp_n(t) - np_{n-1}(t), \quad n \geqslant 1. \tag{49}$$

The corresponding weight coefficients A_i in Eq. (48) are defined by the differential equation with the form

$$A_i = \frac{2}{(1-t_i^2)[p_n'(t_i)]^2}. \tag{50}$$

Generally, the abscissae and weight coefficients of the Gauss–Legendre formula can be computed [62] and tabulated from the Eqs. (49) and (50).

The interval $[-1,1]$ in Eq. (48) can be transformed into a general finite interval $[V_k, V_{k+1}]$. Therefore, the extended Gauss–Legendre quadrature approximation becomes

$$\int_{V_k}^{V_{k+1}} f(V)dV \approx \frac{V_{k+1}-V_k}{2}\sum_{i=1}^{n} A_i f\left(\frac{V_{k+1}-V_k}{2}t_i + \frac{V_{k+1}+V_k}{2}\right). \tag{51}$$

To compute the macroscopic flow moments of the distribution function, the discrete velocity domain $[V_a, V_b]$ in consideration can be subdivided into a sum of smaller subdivisions $[V_k, V_{k+1}]$ with N parts according to the thoughts of the compound integration rule, and then the computation of the integration of the distribution function over the discrete velocity domain $[V_a, V_b]$ can be performed by applying the extended Gauss–Legendre formula (51) to each of subdivisions in the following manner

$$\int_{V_a}^{V_b} f(V)dV = \sum_{k=1}^{N}\int_{V_k}^{V_{k+1}} f(V)dV. \tag{52}$$

3. HPF parallel implementation and efficiency of the gas-kinetic algorithm

It can be shown from the present gas-kinetic algorithm that the DVO method needs to be employed to discretize the molecular velocity space in order to cast the velocity distribution function equation into hyperbolic conservation equations with nonlinear source terms, and then the finite difference method from computational fluid dynamics is developed to numerically solve the velocity distribution functions at each of DVO points. For the computation of three-dimensional flow problems, the six-dimensional array needs to be used to access the discrete velocity distribution functions at all points in the discrete velocity space and physical space, so a great deal of computer memory is needed. On one hand, it is impractical to rely on current serial computer for the present gas-kinetic algorithm to attack three-dimensional complex hypersonic flows. It has been indicated from the computational procedures of the algorithm that, after the physical and velocity space are discretized and the initial condition of the flow field is set as the free-stream equilibrium state, the direct computation of time evolution of the velocity distribution function over the velocity space and physical space can be split up into two parts: one is

that the discrete velocity distribution functions are solved by the gas-kinetic numerical schemes described in Section 2.1 with the use of the gas-kinetic boundary conditions from Section 2.2 independently and concurrently at every given DVO point, the other is that macroscopic flow variables at each point of the physical space are evaluated by the discrete velocity numerical integration methods described in Section 2.3. After the above procedures are finished with the renewed correction of the velocity distribution function equation, the process of the computation of the distribution functions for the new time level will be repeated. The iterative procedure can be stopped when the quadratic global relative error of the flow quantities (e.g. density, flow velocity and temperature) between successive iteration steps is less than 10^{-5}. The essential and important feature of the above-mentioned computation strategy is that the calculations in the velocity space can be uncoupled from those in the physical space without any communication connection, which makes the gas-kinetic algorithm well suitable for parallelizing. To resolve the difficulty of the vast computer memory needed by the current method in solving three-dimensional complex flows and to well exploit massive power of parallel computers, the multi-processing strategy and parallel implementation technique suitable for the gas-kinetic numerical algorithm are investigated by using the technique of domain decomposition.

The computing space of the gas-kinetic algorithm for three-dimensional flow problems relates to the six-dimensional phase space consisting of the discrete velocity space (σ,δ,θ) and physical space (i,j,k). However, none but the velocity distribution function under consideration is defined in the six-dimensional space, while other variables or modules of the algorithm are merely defined in the subspace of (i,j,k) or (σ,δ,θ) in a way that good data-parallel independency exists in the gas-kinetic algorithm. In practical computation, the bounds of the discrete velocity space are wide especially for hypersonic flow problems so that the number of discrete velocity grid points $N_\sigma \times N_\theta \times N_\delta$ needed is quite large, which is specially suitable for the decomposing strategy of discrete velocity space Ω_V. For the domain decomposition of Ω_V, as the computing quantity of the reduced summation spent on the moments of the distribution function is only under 1/5 of the whole computing workload of the algorithm, the number of parallel processors can reach up to the maximum number of $N_\sigma \times N_\theta \times N_\delta$ so that the parallel scalability can be effectively enlarged. Considering that, the computing process of the gas-kinetic algorithm possesses good peculiarity of data parallel, the discrete velocity mesh (σ,δ,θ) will be distributed over the parallel processors in the block-layout manner. To enhance the parallel efficiency, the parallelized loops of σ,δ,θ are adjusted outside the loops of physical coordinates (i,j,k), and so, in this way, the data communication time arisen from the reduced summation during the calculation of macroscopic flow parameters is greatly reduced down to $i_{\max} \times j_{\max} \times k_{\max}$ times. It is found from the parallelizing implementation on the present gas-kinetic algorithm that the workload assigned to each processor for the numerical computation of the $f_{\sigma,\delta,\theta}$ is the $1/n$ of the total computation load, and the size of the distributed memory of each CPU is also the $1/n$ of the total amount of memory in handling the calculation of three-dimensional problems, which makes it possible that the problems unsolved under the limitation of serial computer memory can be attacked by concurrent computation with high parallel efficiency and speed-up ratio. In this study, the HPF parallel code adapted to the present gas-kinetic numerical method has been developed and applied to solve three-dimensional complex flows under the parallel environment offered by the parallel computer from the Parallel Computing Research Center in Beijing.

It has been shown from the computing practice that the results of the present method are not sensitive to the grid spacing in the physical space or the velocity space if only the required precision in the computation can be satisfied. However, the finer is the grid, the slightly better should be the precision of the results for certain at the expense of more computing memory and time. The present method is very stable and robust without the limitation of the cell size, even when the grids are coarse, the computation still is convergent rapidly to the required numerical precision. Fig. 1 describes the converging curve of the present algorithm in solving three-dimensional complex problems, where the vertical-axis denotes the quadratic global residual error of the density and the horizontal abscissa denotes the computing iterative times in the marched time. Generally, for rarefied flow problem, the computational speed of the present method is faster than that of continuum flows. It has been shown from the computations that the computer time required for the present method increases as the Knudsen num-

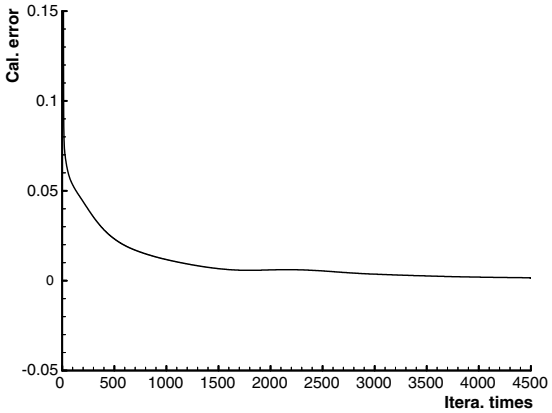

Fig. 1. Converging curve of the present algorithm.

Table 1
Drag coefficients of sphere for $3.8 < M_\infty < 4.3$, $0.006 < Kn_\infty < 0.107$ in the transition flow regime.

$d_s(m)$[a]	0.0191	0.0381	0.0476	0.0381	0.0476	0.0476	0.0572	0.1143	0.1524	0.1523
M_∞[b]	3.865	3.865	3.863	4.169	4.096	4.322	4.324	4.275	4.229	4.322
Kn_∞[c]	0.1071	0.0550	0.0447	0.0350	0.0319	0.0203	0.0163	0.0094	0.0079	0.0064
H(km)[d]	76.525	76.732	76.841	73.522	74.466	71.113	70.828	71.913	72.765	71.180
$C_{D,Exp}$[e]	1.713	1.502	1.452	1.337	1.336	1.275	1.229	1.227	1.206	1.177
$C_{D,Cal}$[f]	1.743	1.491	1.457	1.411	1.389	1.279	1.255	1.233	1.212	1.211
Error(%)[g]	1.75%	0.73%	0.34%	5.53%	3.97%	0.31%	2.12%	0.49%	0.50%	2.89%

[a] Diameter of sphere in meter.
[b] Mach number of the freestream.
[c] Knudsen number of the freestream.
[d] Flying altitude in kilometer corresponding to d_s and Kn_∞.
[e] Drag coefficient from the experiment in Peter and Harry [63].
[f] Drag coefficient from the present computation.
[g] The relative error.

ber decreases. Especially, in the computation of the continuum flow with small Knudsen number, as the molecular mean collision time is generally much less than the allowable time in the CFL stable condition of the finite difference scheme. The computing time step given by Eq. (32), then, will be quite small at the magnitude of 10^{-5}, and, as a result, the convergent speed of the present method becomes slower than the one of the Navier–Stokes solver for the three-dimensional hypersonic continuum flows. For instance, for the current calculation in the ten cases of the sphere flows in the transitional regime shown in Table 1 of Section 4.1, the computing time needed for the convergence is in the range of two hours to five and half hours. However, the present method uses less than one hour to obtain the converged flow distribution shown in Fig. 4 of Section 4.1 for the computation of the high rarefied flow with $Kn_\infty = 1$, $M_\infty = 3$, and takes approximate two days to solve the results of the continuum flow with $Kn_\infty = 0.0001$, $M_\infty = 3$. Moreover, the computing memory required by the present algorithm is greater for complex flows with higher Mach numbers, and more processors and computing time are needed to attain the same precision. In the following computation, 32–512 processors with the distributed memory of 113 Mbytes are used to solve the three-dimensional complex flows with a wide range of Mach numbers from 3 to 19.7.

4. Numerical study of three-dimensional complex flows

In this section, the gas-kinetic numerical algorithm, developed in the foregoing sections, will be used to study the three-dimensional complex flows and the aerodynamic phenomena from rarefied transition to continuum regimes. The cases studied include the hypersonic flow problems around sphere and spacecraft shape with different Mach numbers. In here, the fluid medium is taken as the perfect gas without consideration of the internal energy and chemical reaction, therefore, the internal degrees of freedom are assumed to be in equilibrium with translational degrees of freedom in simulating polyatomic gas flows.

4.1. Three-dimensional sphere flows from rarefied to continuum regime

To investigate the nature of the three-dimensional gas flows, which covers various flow regimes, and to verify the present gas-kinetic numerical models, the basic blunt configuration exemplified by a sphere will be studied and analyzed in detail. A wide range of engineering studies associated with re-entry vehicles are concerned with the aerodynamics of low-density flows in the transitional flow regime between continuum and free-molecule flows. The determination of sphere drag has been for long time a classical problem in aerodynamics. Unfortunately, there are few reliable complete calculations, and careful comparisons between theory and experiment of sphere drag in the transitional flight regime with Reynolds numbers below about 2000. In order to resolve this state of affairs and to gain a comparison with the experimental measurements from Peter and Harry [63], sphere flows with intermediate Mach numbers for $3.8 < M_\infty < 4.3$ are computed under the cases of ten with the sets of $Pr = 0.72$, $T_w/T_0 = 1$, $\gamma = 1.4$, $\chi = 0.75$, where the free-stream Knudsen numbers are in the range of $0.006 < Kn_\infty < 0.107$ with the corresponding free-stream Reynolds number of $50 < Re_\infty < 1000$. To save computer memory with a resource of 32 processors, the space grid points used are only $25 \times 17 \times 21$ with streamwise, circumferential and surface normal directions. The Gauss quadrature formula with the weight function $2/\pi^{1/2}\exp(-x^2)$, described in Section 2.3, is employed in the discrete velocity numerical integration method to determine macroscopic flow parameters. Table 1 illustrates the computed results of the drag coefficients of the sphere with the comparison of the experimental data [63]. Each column, from the second to the eleventh, respectively refers to the simulation of ten cases: the parameters including the diameter d_s of the sphere, the Mach number M_∞ and Knudsen number Kn_∞ of the freestream in the front three rows of that column are given from the experiment Ref. [63] and are used as input to the simulation code, and the values below are output. To provide physical insight concerning the flying states of transitional flows, the flying altitude H(km) of the sphere relative to the given free-stream Knudsen number Kn_∞ and the diameter d_s of the sphere are educed with the range of 70 km < H < 77 km and also shown in the fourth row of Table 1. It is seen from Table 1 that the computed drag coefficients,

in the sixth row, are in excellent agreement with the experimental data indicated in the fifth row with all of Knudsen numbers from $Kn_\infty = 0.1071$ to $Kn_\infty = 0.0064$. The relative differences denoted in the seventh row are of the order of 0.31–5.53%, which indicates that the present algorithm has good capability in computing the aerodynamics of the rarefied transitional flow even though the coarse spatial mesh system is used. To analyze and compare the flow structures past the sphere with the DSMC solutions from [64], the flow state of $Kn_\infty = 0.03$, $M_\infty = 3.83$, $Pr = 2/3$, $T_w/T_0 = 1$, $\gamma = 5/3$, $\chi = 0.75$ from the near-continuum transitional regime is studied. Fig. 2 shows the variation of temperature and flow velocity on the stagnation line in front of the body, where the vertical ordinate of $(T - T_{oo})/(T_o - T_{oo})$ and U/V_{oo}, respectively denote the non-dimensionalized temperature $(T - T_\infty)/(T_o - T_\infty)$ and velocity $|\bar{U}|/V_\infty$ distribution, and the abscissa denotes the non-dimensionalized position from the stagnation point in the direction of the freestream. As shown in Fig. 2, the computed profiles agree with the DSMC results [64], however, some difference appears in the temperature profiles from Fig. 2(a), as seems to result from the considerable statistical scatter of the DSMC results. For the comparison of the drag coefficient of the above-mentioned sphere, the present computed value of $C_{D,Cal} = 1.3749$ is in good agreement with the DSMC result of $C_{D,DSMC} = 1.4122$ with the relative deviation of 2.64%, even though the present computation is performed in quite a coarse spatial mesh system of $25 \times 19 \times 27$, as indicates that the present algorithm is not sensitive to spatial grid division with strong and stable capability of computing convergence.

Rarefied hypersonic flows about bodies are of greatest practical interest. The hypersonic flows in the near-continuum transitional regime are difficult to treat either experimentally or theoretically over an altitude range of 40–90 km. To illustrate the capability of the present gas-kinetic numerical method for hypersonic Mach number flows and to apperceive the physical nature of hypersonic transition flows, eight cases of hypersonic flows past sphere are computed with the sets of $Pr = 0.72$, $T_w = 300k$, $\gamma = 1.4$, $\chi = 0.75$ with different Reynolds numbers Re_2 behind the wave and Mach numbers of $M_\infty = 8.65$, 8.68, 10.39, 13 from the low-density wind tunnel test conditions of Koppenwallner and Legge [3]. Table 2 summarizes the computing parameters of the above states, where each column from the second to the ninth respectively refers to the flow state of eight cases, parameters, including the diameter d_s of the sphere, the Mach number M_∞ of the freestream and the Reynolds number Re_2 behind the normal wave in the front three rows of that column, are given from the experiment Ref. [3] and are also used as input to the simulation code. The other values in the back three rows including the free-stream Knudsen numbers (Kn_∞), Reynolds numbers (Re_∞) and the relevant flight altitudes H(km) are obtained from the computa-

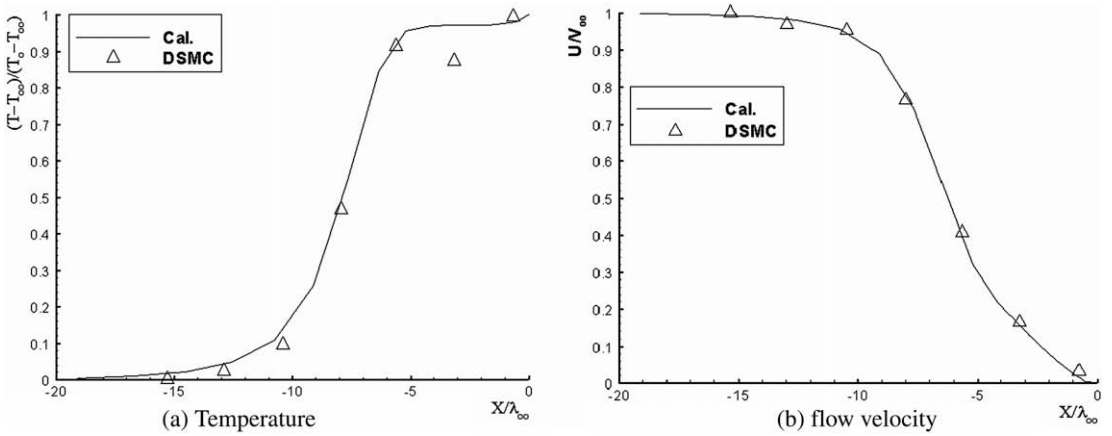

Fig. 2. Stagnation-line profiles for a sphere with $Kn_\infty = 0.03$, $M_\infty = 3.83$, where X/λ_∞ is the distance from the stagnation point of body surface. Solid line, present computations; delta, DSMC results [64].

Table 2
Computed states of hypersonic flows of $M_\infty = 8.65$, 8.68, 10.39 and 13 past sphere for $0.005 \leqslant Kn_\infty \leqslant 8.266$, 58 km < H < 85 km, $1.5 < Re_\infty < 3950$.

$d_s(m)$[a]	0.04	0.04	0.04	0.005	0.003	0.001	0.001	0.001
M_∞[b]	13.00	13.00	13.00	10.39	8.68	8.65	8.65	8.65
Re_2[c]	271.53	191.61	113.60	23.62	10.093	3.3996	0.9926	0.1985
Kn_∞[d]	0.0050	0.0071	0.0119	0.0640	0.1616	0.4827	1.6532	8.2659
Re_∞[e]	3943.13	2782.54	1649.69	245.32	131.11	27.07	7.90	1.58
H (km)[f]	58.07	60.96	65.44	62.01	61.45	65.55	75.07	84.79

[a] Diameter of sphere in meters.
[b] Mach number of the freestream.
[c] Reynolds number behind the normal shock.
[d] Knudsen number of the freestream related to M_∞ and Re_2.
[e] Reynolds number of the freestream.
[f] Flying altitude in kilometer related to d_s and Kn_∞.

tion. It can be shown from Table 2 that the flying altitude corresponding to the considered eight cases is in the range of 58 km < H < 85 km and the free-stream Knudsen number is in the wide range of $0.005 < Kn_\infty < 8.266$ with $1.5 < Re_\infty < 3950$ relative to the small characteristic length of sphere diameter. The computed results of the drag coefficients as a function of the free-stream Knudsen numbers are shown in Fig. 3 together with the early experimental data [3]. In this case, the abscissa (Kn) denotes the logarithm values of Kn_∞, and the vertical ordinate denotes the drag coefficient (C_D) of sphere. In general, the agreement between the present computations and the experiments can be observed well. Fig. 4 shows the flow field contours of Mach number, temperature and flow velocity in the symmetrical plane around the sphere corresponding to the aforementioned flow states of (a) $Kn_\infty = 1.6532$, $M_\infty = 8.65$, (b) $Kn_\infty = 0.064$, $M_\infty = 10.39$ and (c) $Kn_\infty = 0.0071$, $M_\infty = 13$, where the numeral on the contours denotes the normalized magnitude of related flow parameters. It can be indicated from Fig. 4 that the flow decelerates gradually as it approaches the body. The disturbed region of flow becomes wider for the full rarefied flow with higher Knudsen number of $Kn_\infty = 1.6532$. The disturbed zone of the blurry shock wave appears in front of the body for the rarefied transitional flow of $Kn_\infty = 0.064$, and in the end, a thick and explicit bow shock wave is formed so that the flow field is clearly divided into the undisturbed gas and the disturbed one in the hypersonic near-continuum flow of $Kn_\infty = 0.0071$, $M_\infty = 13$. Furthermore, it exists a zone of high temperature in the contours of temperature due to the cooled body with low surface temperature, the hypersonic flow around the body passes by the zenith with the supersonic expansion, and there does not form any recompression phenomena in the back of the body.

To numerically analyze the flow features and physical nature from various flow regimes and to test the reliability of the present gas-kinetic algorithm in solving three-dimensional flow problems from rarefied transition to continuum regime, four cases of the $M_\infty = 3$ flow past sphere with $Kn_\infty = 1$, 0.1, 0.01 and 0.0001, $Pr = 2/3$, $T_w/T_0 = 1$, $\chi = 0.75$ are investigated by the HPF parallel computation. In this instance, the modified Gauss-type quadrature method for the discrete velocity space is employed with the $41 \times 21 \times 35$ spatial cells in the physical space. It can be shown from the flow velocity contours, in Fig. 5, that for the fully rarefied flow related to $Kn_\infty = 1$, the disturbed region of flow is quite large and the flow decelerates gradually clinging to the body surface as it approaches the sphere. As the Knudsen number decreases from $Kn_\infty = 1$ to $Kn_\infty = 0.0001$, the disturbed region of flow becomes smaller and smaller near the body, and the strong disturbance, the dim bow shock and the recompression phenomena of the flow, appear in the rarefied transition flows related to $Kn_\infty = 0.1$ and $Kn_\infty = 0.01$. For the supersonic continuum flow of $Kn_\infty = 0.0001$, the flow structures including the thin front bow shock, the stagnation region, the accompanied weak shock wave beyond the top of sphere, the recompressing shock wave formed by the turning of the flow and the wake region are captured well. Furthermore, the front bow shock wave is closer to the body when the flow approaches the continuum flow from the near-continuum transition flow by diminishing the Knudsen number from $Kn_\infty = 0.1$ to $Kn_\infty = 0.0001$. The streamline structures in the symmetrical plane around sphere for the cases of $Kn_\infty = 0.1$, $Kn_\infty = 0.01$ and $Kn_\infty = 0.0001$ are shown in Fig. 6, where the arrowhead on the streamline denotes the flow direction, and the symbol (Kn) in all of figures denotes the free-stream Knudsen number (Kn_∞). It can be seen that for rarefied transitional flows of $Kn_\infty = 0.1$ and $Kn_\infty = 0.01$, the flow is attached to the sphere surface with strong wall slip effect of flow velocity, and there is no evidence of flow separation in the wake, as is expected for this two rarefied flow conditions of $Re_\infty = 43.67$ and $Re_\infty = 436.67$. However, for the case of $Kn_\infty = 0.0001$, the boundary layer flow separation behind the sphere is clearly visible and the separated vortices exist in the wake with well defined recirculation zones as the feature of the continuum flow. The flow details of the boundary layer separation, the separated vortex, and the near wake will be stable for this flow with the Reynolds number of $Re_\infty = 43666.96$. Fig. 7 qualitatively reveals the variation of collision frequency with different position points in the interior of the flow field for various flow regimes from $Kn_\infty = 1$ to

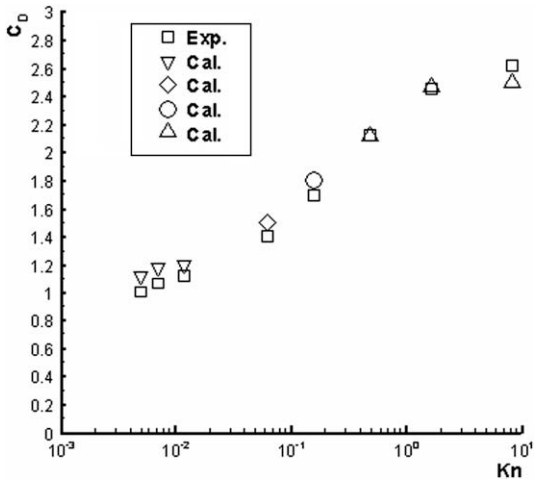

Fig. 3. Drag coefficients for hypersonic flow past a sphere. Square (□) represents experimental data in Koppenwallner and Legge [3]; other symbols denote the present computed results, where gradient (▽) corresponds to $M_\infty = 13$, diamond (◇) corresponds to $M_\infty = 10.39$, circle (○) corresponds to $M_\infty = 8.68$, delta (△) corresponds to $M_\infty = 8.65$.

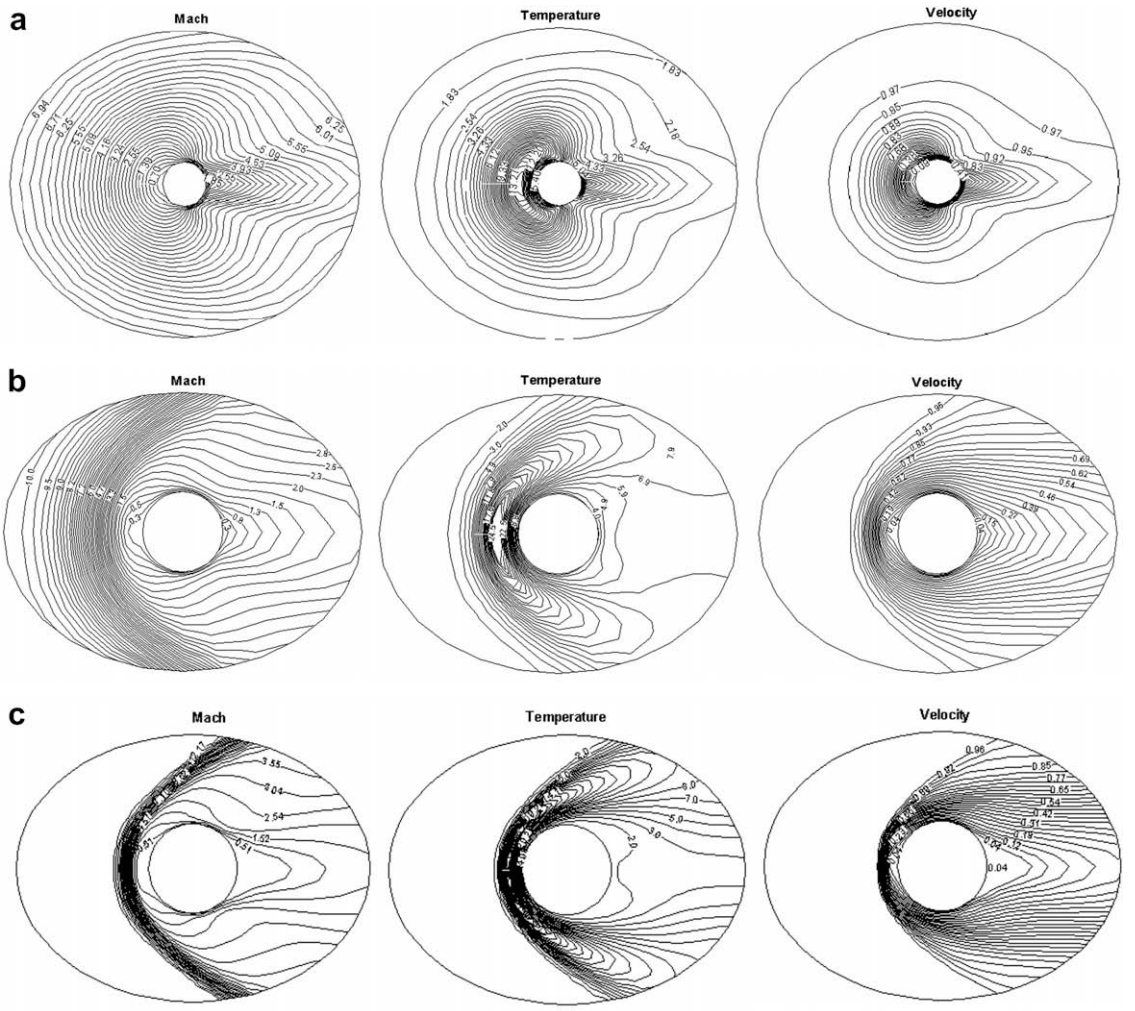

Fig. 4. Mach number, temperature and flow velocity contours of hypersonic flows past sphere for (a) $Kn_\infty = 1.6532$, $M_\infty = 8.65$, (b) $Kn_\infty = 0.064$, $M_\infty = 10.39$ and (c) $Kn_\infty = 0.0071$, $M_\infty = 13$.

$Kn_\infty = 0.0001$. It can be illustrated that the collision frequency is entirely different with variation of spatial position in the flow field around the body. For the completely rarefied flow of $Kn_\infty = 1$, $M_\infty = 3$, the intermolecular collisions are quite rare, the collision frequency just varies from a maximum of about 4.92 near the stagnation point to the minimum value of 10^{-3} near the back-end of the body in the wake region. However, in the rarefied transition flows of $Kn_\infty = 0.1$ and $Kn_\infty = 0.01$ or continuum flow of $Kn_\infty = 0.0001$, the gas becomes more and more dense, the collision frequency rapidly increases and the strong disturbance and bow shock wave appears. Particularly for the case of $Kn_\infty = 0.0001$, $M_\infty = 3$, the collision frequency varies from a maximum of about 71345.2 near the stagnation point to a minimum value of less than 630 in the wake. Fig. 8 presents the stagnation line profiles of pressure for the cases of $Kn_\infty = 0.1$, $Kn_\infty = 0.01$ and $Kn_\infty = 0.0001$, respectively. For the supersonic rarefied flow of $Kn_\infty = 0.1$, $M_\infty = 3$, the pressure rises smoothly and gradually and goes up to the maximum value at the sphere stagnation point as the flow approaches the sphere, which forms a quite wide region of flow disturbance. However, for the near-continuum transition flow with a low Knudsen number of $Kn_\infty = 0.01$, the region of pressure disturbances almost cuts down to half of that for the case of $Kn_\infty = 0.1$, and there exists the faint shock wave in the stagnation-line profiles. For the supersonic continuum flow of $Kn_\infty = 0.0001$, $M_\infty = 3$, the sharp variation of pressure only occurs in the very narrow disturbed domain so much as half of that in the case of $Kn_\infty = 0.01$, and a thin and clear shock wave lies in the stagnation-line near the forepart of the body. Figs. 5–8 qualitatively reveal the evolving process and physical phenomena of the flows around the body from the highly rarefied to continuum flow while the Knudsen number diminishes from $Kn_\infty = 1$ to $Kn_\infty = 0.0001$.

Since the present gas-kinetic algorithm explicitly evaluates the time evolution of the molecular velocity distribution function to update all the macroscopic flow variables, it is different from any other numerical approach where the macroscopic fluid equations are discretized directly, and the slip boundary condition can be naturally comprised and satisfied according

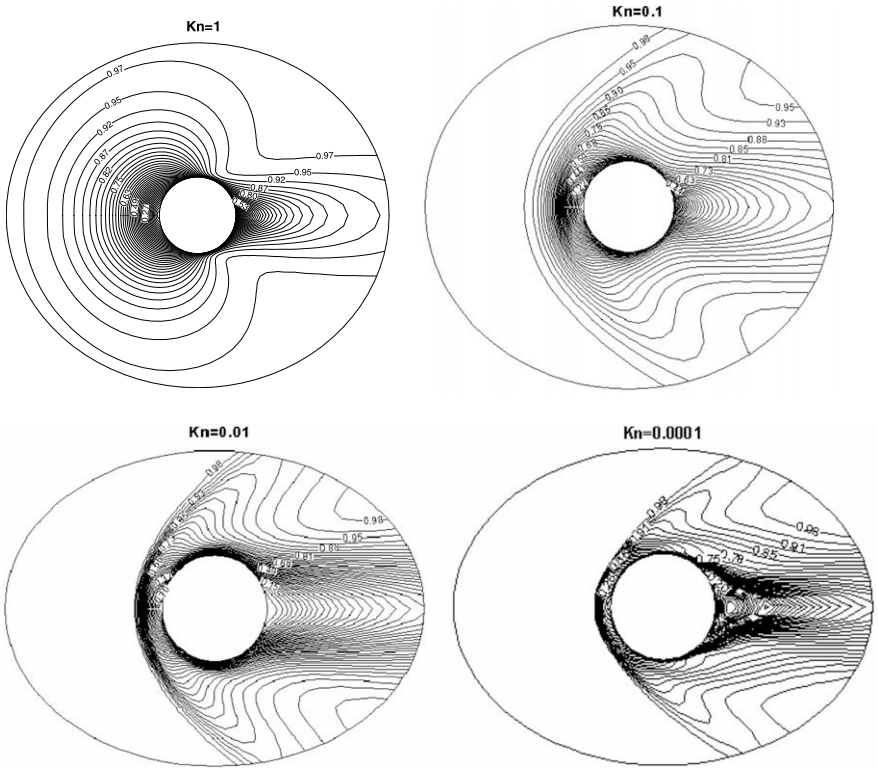

Fig. 5. Flow velocity contours in the symmetrical plane around sphere for $Kn_\infty = 1$, 0.1, 0.01 and 0.0001 with $M_\infty = 3$.

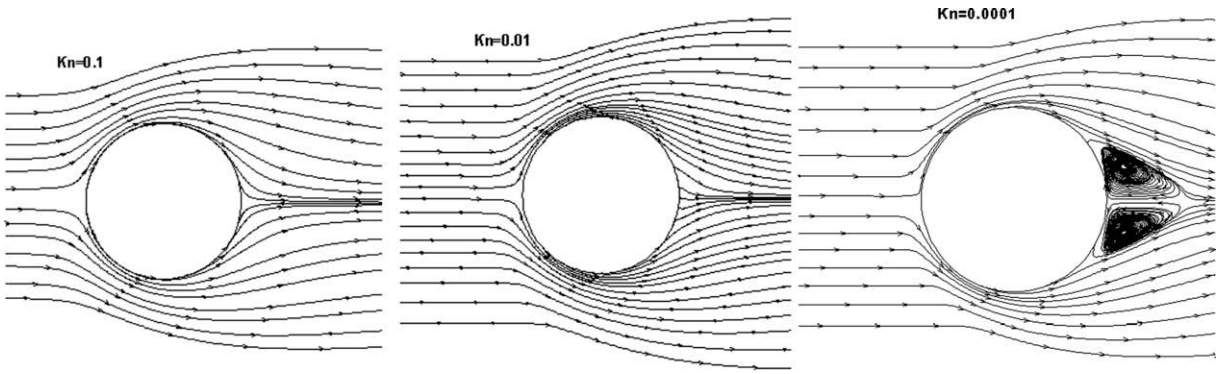

Fig. 6. Streamlines in the symmetrical plane around sphere for $Kn_\infty = 0.1$, 0.01 and 0.0001 with $M_\infty = 3$.

to the interaction model between the gas and the solid surface. To explore the wall slip phenomena from various flow regimes and flow details along the body surface, Fig. 9 illustrates the normalized tangent velocity (V_t/V_∞), that is so-called wall slip velocity, along the sphere surface in the cases of $Kn_\infty = 0.1$, 0.01 and 0.0001. For the continuum flow with the very low Knudsen number of $Kn_\infty = 0.0001$, the tangent velocity along the body surface is quite small particularly near the region of the stagnation point so that it can be neglected, which is consistent with the assumption of no slip velocity of macroscopic continuum fluid dynamics. However, even though for the case of $Kn_\infty = 0.0001$ and $M_\infty = 3$, the slip velocity still gradually goes up to the maximum value of about 0.0428 in the region far from the stagnation point, especially beyond the top of the sphere. As the free-stream Knudsen number increases along with augmentation of the effect of gas rarefaction, the magnitude of slip velocity increases rapidly. For the near-continuum flow of $Kn_\infty = 0.01$ and the rarefied transitional flow of $Kn_\infty = 0.1$, on almost all of the body surface exists wall slip phenomena except the front and back stagnation point, particularly for the case of $Kn_\infty = 0.1$, the maximum value of wall slip velocity almost reaches to half of the free-stream velocity, that is about $(V_t/V_\infty)_{max} = 0.4296$.

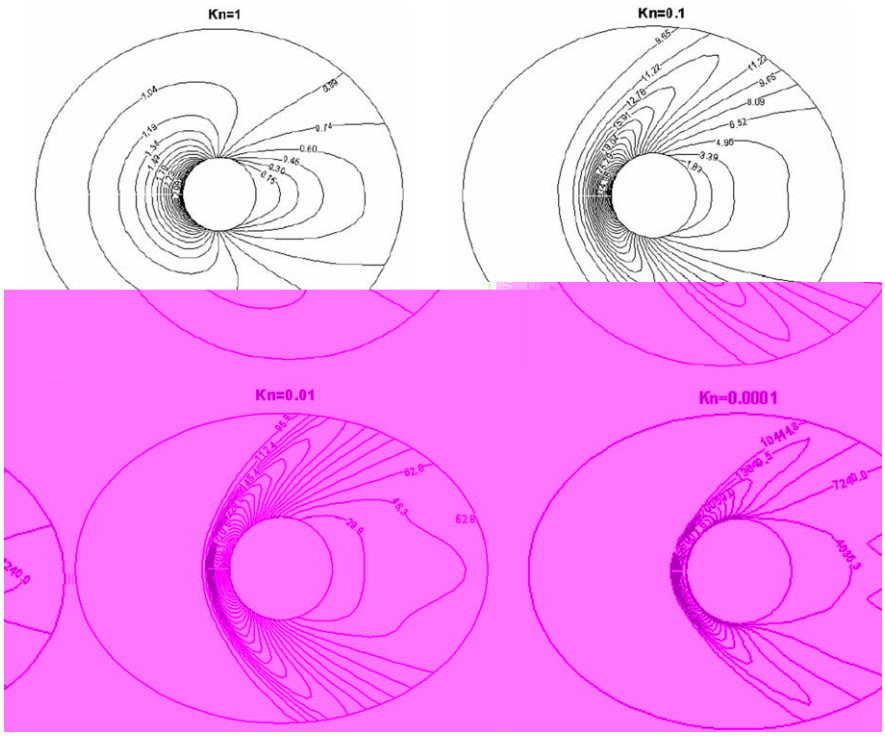

Fig. 7. Variation of collision frequency in the symmetrical plane around sphere for $Kn_\infty = 1$, 0.1, 0.01 and 0.0001 with $M_\infty = 3$.

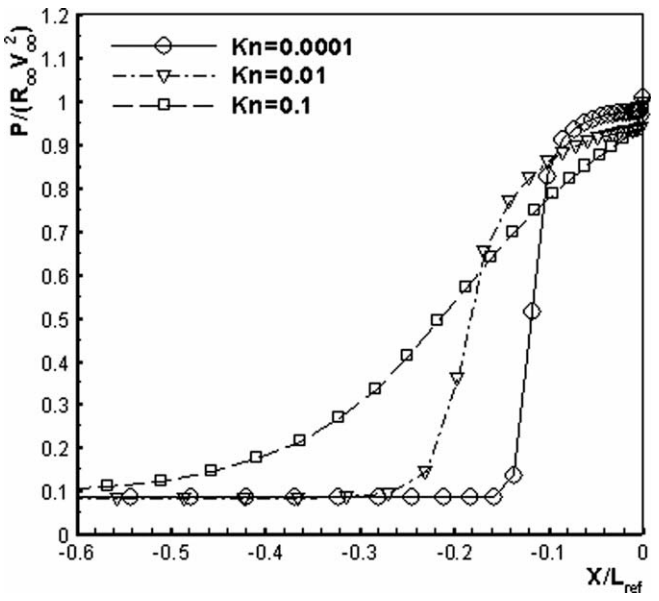

Fig. 8. Stagnation-line pressure profiles of a sphere for $Kn_\infty = 0.1$, 0.01 and 0.0001 with $M_\infty = 3$, where abscissa (X/L_{ref}) is the normalized distance from body surface based on the diameter of sphere, and coordinate $(P/(R_{oo}V_{oo}^2))$ denotes the normalized pressure $(p/(\rho_\infty V_\infty^2))$.

4.2. Hypersonic flow problems past spacecraft shape

In this subsection, we apply the gas-kinetic algorithm to study three-dimensional complex flows past the spacecraft shape with various Knudsen numbers and Mach numbers. Figs. 10 and 11, respectively present the computed results of Mach number and pressure contours for the two cases of $Kn_\infty = 0.5$ and $Kn_\infty = 0.01$ with $M_\infty = 5$, $\alpha = 20°$, $Pr = 0.72$, $T_w/T_0 = 1$, $\gamma = 1.4$. It can be shown that for the near-continuum flow of $Kn_\infty = 0.01$, the flow structures including the front bow shock, stagna-

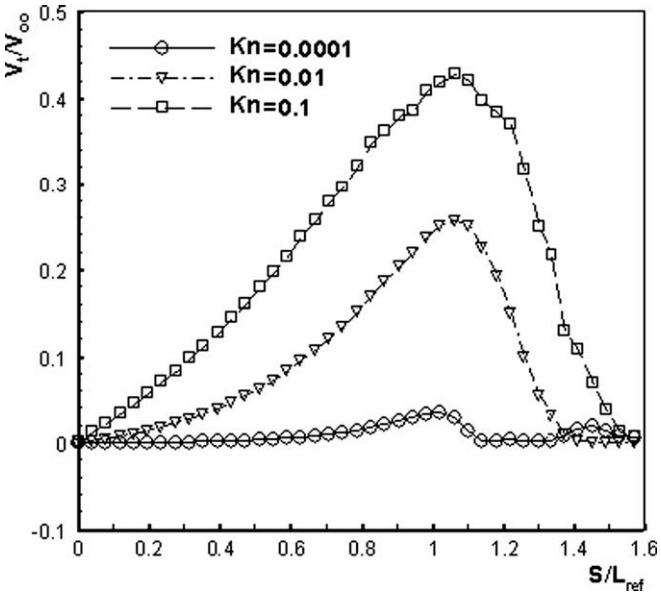

Fig. 9. Slip velocity along the tangent direction of sphere surface for $Kn_\infty = 0.1$, 0.01 and 0.0001 with $M_\infty = 3$, where abscissa (S/L_{ref}) is the normalized surface distance from the stagnation point based on the diameter of sphere, and coordinate (V_t/V_{oo}) denotes the normalized tangent velocity V_t/V_∞.

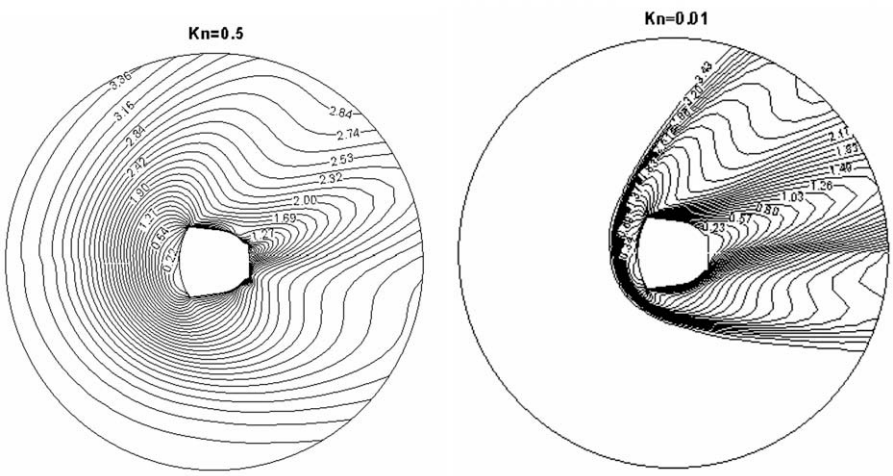

Fig. 10. Mach number contours in the symmetrical plane past spacecraft shape for $Kn_\infty = 0.5$ and $Kn_\infty = 0.01$ with $M_\infty = 5$ and $\alpha = 20°$.

tion region and recompression shock are well captured, however, for the highly rarefied flow of $Kn_\infty = 0.5$, there exists the wide domain of flow disturbance around the body with no shock wave and recompression phenomena in the flow field. Figs. 10 and 11 qualitatively reveal that the gas flow gradually approaches from highly rarefied flow to near-continuum flow while the Knudsen number diminishes from $Kn_\infty = 0.5$ to $Kn_\infty = 0.01$.

To reveal the variation of stagnation line profiles from various flow regimes, Fig. 12 shows the flow velocity distribution past the spacecraft shape along with the stagnation line for the full rarefied flow of $Kn_\infty = 5$, $M_\infty = 4$ and the near-continuum flow of $Kn_\infty = 0.01$, $M_\infty = 4$. In the rarefied flow regime, the flow velocity smoothly and gradually increases from the zero at the stagnation point to the free-stream value near the undisturbed outer boundary for the case of $Kn_\infty = 5$, $M_\infty = 4$, which undergos a wider region of disturbed flow up to many times of the characteristic length of the body. However, in the near-continuum transitional flow regime, the flow velocity almostly approximates to zero in the vicinity of the stagnation point, and at some distance far from the stagnation point, the flow velocity sharply goes up with distinctly jumping phenomena, then approaches the free-stream value corresponding to the near-continuum flow of $Kn_\infty = 0.01$, $M_\infty = 4$. It is indicated from Fig. 12(b) that the flow phenomena of the front bow shock wave is in a very narrow disturbed domain less than two fifth of the characteristic length. Fig. 13 shows the normalized wall velocity components U/V_∞ and V/V_∞ in the symmetrical

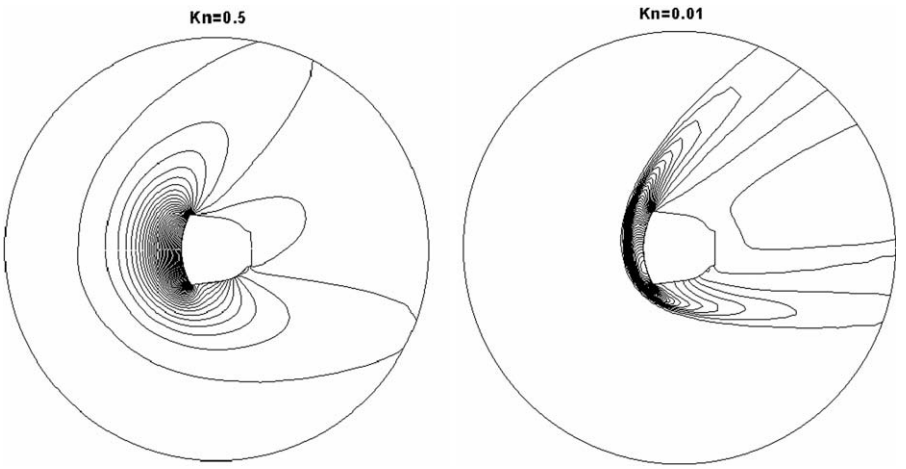

Fig. 11. Pressure contours in the symmetrical plane past spacecraft shape for $Kn_\infty = 0.5$ and $Kn_\infty = 0.01$ with $M_\infty = 5$ and $\alpha = 20°$.

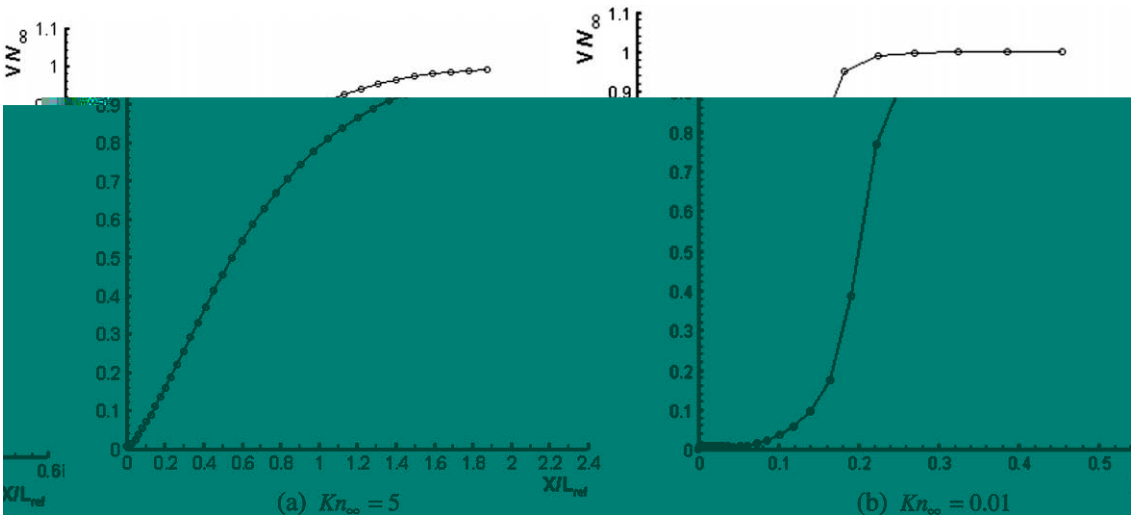

Fig. 12. Stagnation line velocity profiles from different flow regimes for $Kn_\infty = 5$ and $Kn_\infty = 0.01$ with $M_\infty = 4$, where abscissa (X/L_{ref}) is the normalized distance from the stagnation point of the body, and coordinates (V/V_{oo}) denote the normalized flow velocity $|\vec{U}|/V_\infty$.

plane along the body surface from the stagnation point related to the two cases of $Kn_\infty = 5$ and $Kn_\infty = 0.01$ with $M_\infty = 4$, $\alpha = 0°$. It can be revealed that the wall velocity diminishes down to zero in the vicinity of the front and back stagnation point. However, a distinct wall slip velocity exists far from the stagnation point both for the high rarefied flow of $Kn_\infty = 5$ and for the near-continuum flow of $Kn_\infty = 0.01$. While the free-stream Knudsen number increases from $Kn_\infty = 0.01$ to $Kn_\infty = 5$, the effect of gas rarefaction is greatly enhanced, which induces that the wall slip velocity increases rapidly so that the maximum value of the wall slip velocity is more than half of the free stream velocity for the case of $Kn_\infty = 5$, $M_\infty = 4$. To reveal the varying characteristic of surface heat flux covering various flow regimes, Figs. 14 and 15, respectively show the distribution of heat flux $q/(\rho_\infty a_\infty^3)$ along the streamwise surface of the spacecraft for two cases of $Kn_\infty = 5$, $M_\infty = 4$, $\alpha = 0°$ and $Kn_\infty = 0.001$, $M_\infty = 4$, $\alpha = 20°$, where the horizontal coordinates denote the surface distance S/L_{ref} from the front end point of the body along stream direction. It can be shown from Fig. 14 corresponding to the full rarefied flow of $Kn_\infty = 5$, $M_\infty = 4$, with $\alpha = 0°$ that the maximum value of surface heat flux appears at the front end point of the body, the surface heat flux descends gradually along with the variation of surface curvature, and the surface heat flux goes sharply down across the top of the body, then holds the line on the whole in course of the surface of the inversion cone, ultimately drops down to zero in the leeward region of the spacecraft, which reflects the peculiarity of attaching wall flow in the high rarefied flow regime. Fig. 15 shows the distribution of the surface heat flux along with the three symmetrical meridian planes of $\varphi = 0°$, 90°, 180° related to the case of supersonic continuum flow of $Kn_\infty = 0.001$, $M_\infty = 4$, $\alpha = 20°$. For the windward plane of $\varphi = 0°$, the surface heat flux gradually goes up and reaches the maximum value at the top of the body; however for the cross-stream plane of $\varphi = 90°$ and the leeward plane of $\varphi = 180°$ the maximum heat flux arises at the front end point of the body. In the region of

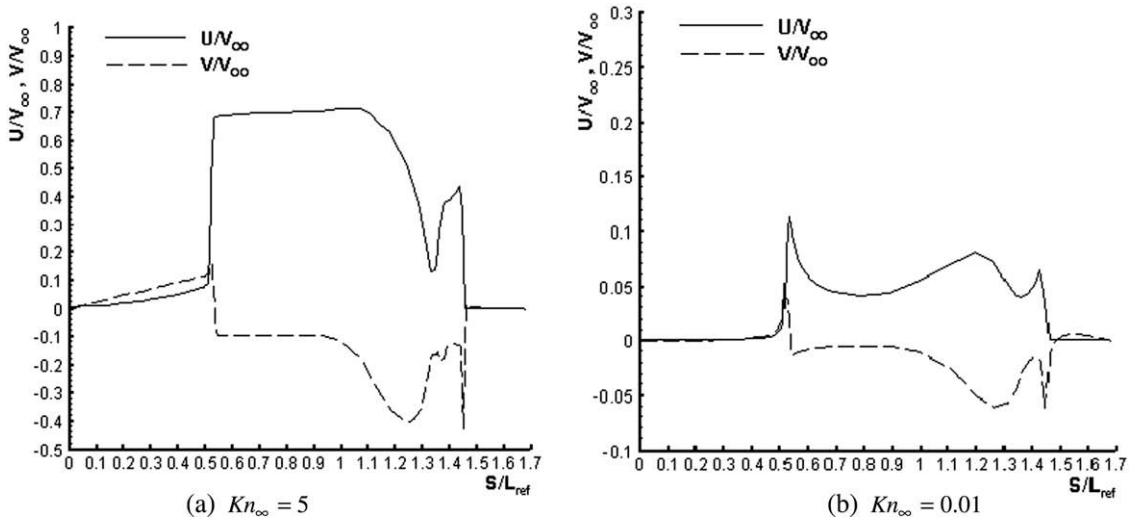

Fig. 13. Axial and lateral flow velocity distribution along the body surface in the symmetric plane around the spacecraft shape for $Kn_\infty = 5$ and $Kn_\infty = 0.01$ with $M_\infty = 4$ and $\alpha = 0°$, where abscissa (S/L_{ref}) is the normalized surface distance from the forefront point of the body, and coordinates (U/V_{oo},V/V_{oo}) denote the normalized flow velocity U/V_∞ and V/V_∞ in axial and lateral direction, respectively.

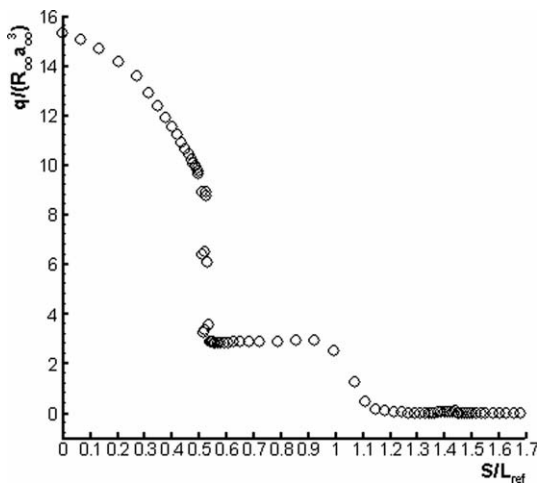

Fig. 14. Heat flux distribution along the body surface past spacecraft shape for $Kn_\infty = 5$, $M_\infty = 4$ and $\alpha = 0°$, where abscissa (S/L_{ref}) is the normalized surface distance from the forefront point of the body, and coordinate $q/(R_{oo}a_{oo}^3)$ denotes the magnitude of normalized heat flux $q/(\rho_\infty a_\infty^3)$.

the afterbody across the top of the body, the surface heat flux goes sharply down owing to the rapid expansion of the flow so that the heat flux turns to the minimum in the back end of the body. It can be validated from Figs. 14 and 15 that the surface heat flux for the full rarefied flow of $Kn_\infty = 5$, $M_\infty = 4$ is six times as much as that for the near-continuum flow of $Kn_\infty = 0.001$, $M_\infty = 4$.

To numerically analyze and compare the variation of flow pattern, from rarefied to continuum regime around three-dimensional complex bodies, Fig. 16 shows the vector streamline structures around the spacecraft shape for the three cases of $Kn = 5$, $Kn = 0.01$ and $Kn_\infty = 0.001$ with $M_\infty = 4$ under different angles of attack $\alpha = 0°$ and $\alpha = 20°$. It can be seen that for high rarefied flow of $Kn = 5$, it is completely attached to the surface with strong wall slip effect and there is no evidence of flow separation in the back of the body. However, in the near-continuum transition flow with low Knudsen number of $Kn = 0.01$, the flow separation and vortex wake structures emerge from the rearward region of the body. For the case of supersonic continuum flow with $Kn_\infty = 0.001$, $M_\infty = 4$, the boundary layer flow separation in the region of the afterbody is clearly visible and the separated vortex exists in the wake with a well defined recirculation zone, as it is only a particular feature of continuum gas flow. The above computations nicely tally with the theoretical predictions and applicable test.

Finally, to solve the problem of the trim angle of attack of the re-entry flight, we compute and study the flying states of hypersonic Mach number flow past the spacecraft shape for the flying case of $Kn_\infty = 0.0063$, $M_\infty = 15.587$, $Re_\infty = 3729.15$ and $T_w/T_0 = 0.5435$. Fig. 17(a) illustrates the Mach number contours in the symmetrical plane past the body with the flying angle

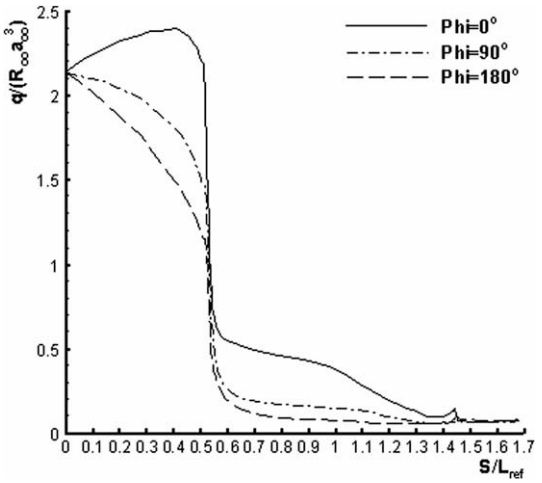

Fig. 15. Heat flux distribution along the body surface in different meridian planes of $\varphi = 0°$, 90°, 180° past spacecraft shape for $Kn_\infty = 0.001$, $M_\infty = 4$ and $\alpha = 20°$.

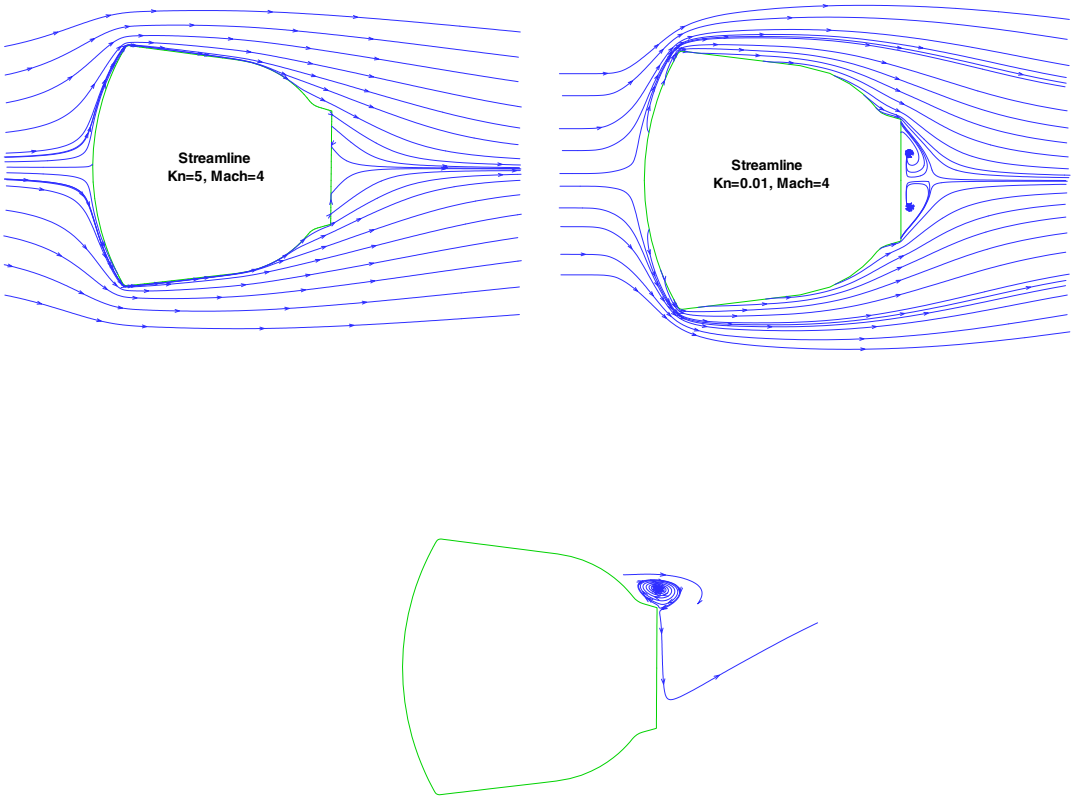

of attack of $\alpha = 26°$. It can be observed from Fig. 17(a) and the above-mentioned Figs. 4, 5 and 10 that no recompression shock exists in the hypersonic flows around the body, which exhibits the flow characteristic remarkably different from supersonic

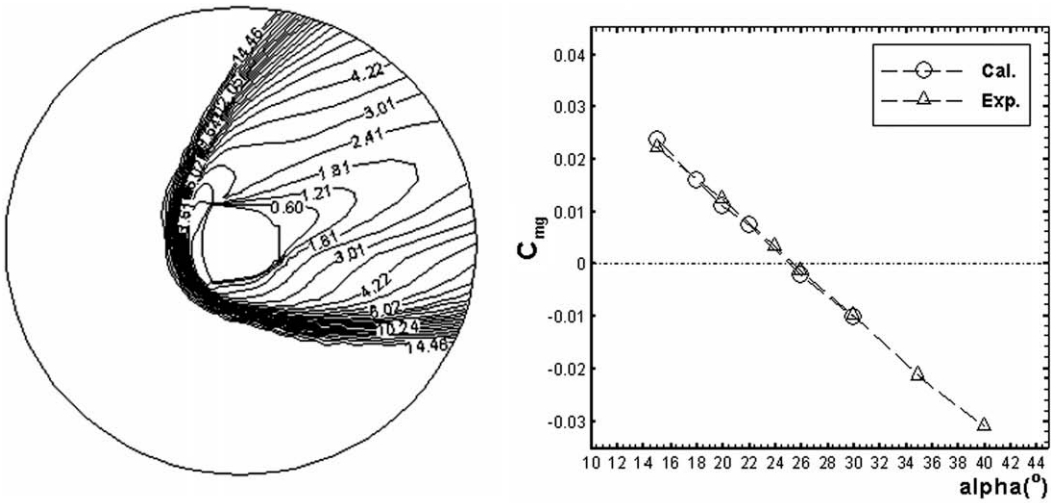

(a) Mach number contours with $\alpha = 26°$ (b) Pitching moment coefficient C_{mg} vs $\alpha(°)$

Fig. 17. Hypersonic flow past spacecraft shape for $Kn_\infty = 0.0063$, $M_\infty = 15.587$, $Re_\infty = 3729.15$.

flows, and that the hypersonic flow generally expands supersonically beyond the top of the body and remains supersonic in most of the wake region. Fig. 17(b) presents the pitching moment coefficient C_{mg} relative to the centre of mass as a function of angle of attack α for the relevant flight altitude of $H = 88.34$ km, where the symbols of circle ($\circ$) denote the present computed results for $\alpha = 15°, 18°, 20°, 22°, 26°, 30°$ and the delta (Δ) corresponds to the experimental data [65] from low-density hypervelocity wind tunnel. It can be shown from the comparison that the present computations of C_{mg} are in good agreement with the experiments, where the computed trim angle of attack is $\alpha_{Cal} = 25.06°$ and the experimental measurement is about $\alpha_{Exp} = 25.39°$. To further study the flying flow problem of the spacecraft shape in high rarefied flow regime, the hypersonic flow state for the case of $Kn_\infty = 1.3417$, $M_\infty = 19.7$, $Re_\infty = 22.18$ with the flight altitude of $H = 120$ km is computed. Fig. 18(a) presents the Mach number contours in the symmetric plane past the body with the angle of attack of $\alpha = 30°$. It can be shown from Fig. 18(a) that it exists a large disturbed region of flow with the strong compressing phenomena in front of the body, which is completely different from the near-continuum transitional flow depicted in Fig. 17(a). Furthermore, the computed trim angle of attack can be obtained as $\alpha_{Cal} = 39.5°$ from Fig. 18(b), where the pitching moment coefficient C_{mg} is plotted as a function of angle of attack α with $\alpha = 10°, 15°, 20°, 25°, 35°$, and $48°$. The above computations are nicely consistent with the theoretical prediction and applicable test.

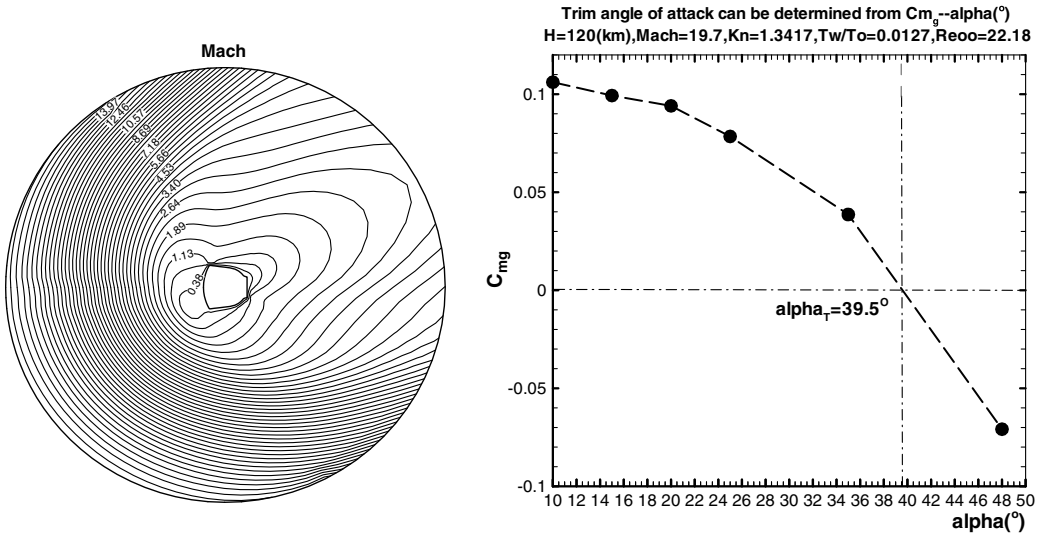

(a) Mach number contours with $\alpha = 30°$ (b) Pitching moment coefficient C_{m_g} vs $\alpha(°)$

Fig. 18. Hypersonic rarefied flow past spacecraft shape for $Kn_\infty = 1.3417$, $M_\infty = 19.7$, $Re_\infty = 22.18$.

5. Concluding remarks

In this paper, the gas-kinetic numerical algorithm is studied and developed to solve the three-dimensional complex problems concerning hypersonic flows of spacecraft re-entry into the atmosphere in perfect gas. The present numerical method studies and uses the non-linear Boltzmann model equation describing molecular transport phenomena from various flow regimes as the starting point for the computation, the single velocity distribution function equation is transformed into hyperbolic conservation equations with non-linear source terms by introducing the DVO method of gas kinetic theory. The time-splitting method for the unsteady equation is used to split up the discrete velocity distribution function equations into the colliding relaxation equations and the convective movement equations, the NND finite difference scheme is employed to solve the convective equations and the second-order Runge–Kutta method is used to numerically simulate the colliding relaxation equations. Then, the gas-kinetic finite-difference numerical scheme directly solving the velocity distribution function is constructed for the three-dimensional complex flows. The gas-kinetic boundary conditions are studied and numerically implemented in the gas-kinetic scheme by directly acting on the velocity distribution function. The specific Gauss-type numerical integration methods, such as the Gauss quadrature formulas with the weight function $2/\pi^{1/2}\exp(-V^2)$ and the Gauss–Legendre composite quadrature technique, are developed and applied to simulate three-dimensional hypersonic flows. As a result, the gas-kinetic numerical algorithm is founded to solve the three-dimensional complex flows with high Mach numbers covering the full spectrum of flow regimes from the view of mesoscopic theory by directly tracing the time evolution of the velocity distribution function, which is completely different from molecular particle transport methods or macroscopic fluid dynamics solvers.

By HPF parallel computing, the present gas-kinetic algorithm has been employed to study the three-dimensional hypersonic flows and aerodynamic phenomena around sphere and spacecraft shape with different Knudsen numbers and Mach numbers covering various flow regimes. The computed results match the relevant experimental data and DSMC results well, and the peculiar flow phenomena and mechanisms from various flow regimes are explored. In the current gas-kinetic numerical method, numerically it becomes more robust and convenient to solve the single velocity distribution function equation rather than the various-order terms in the macroscopic fluid equation, and all macroscopic flow variables are evaluated simply by the moments of the velocity distribution function. It can be tested from this study that the gas-kinetic numerical algorithm directly solving the Boltzmann simplified velocity distribution function equation may provide an important and feasible way that complex hypersonic aerothermodynamic problems and flow mechanisms from rarefied transition to continuum flow regimes can be effectively studied with the aid of the power of modern parallel computer systems. As this work is only the beginning of a gas-kinetic numerical study of hypersonic flows by solving the Bolzmann-type velocity distribution function equation, further investigations on the kinetic models for multi-component real gas effects involving internal energy, chemical reaction, and the efficiency and improvement of the present method, etc., need to be studied in more detail.

Acknowledgments

This work was supported by the National Nature Science Foundation of China under Grants Nos. 90205009 and 10321002, and the National Parallel Computing Center in Beijing. The authors are particularly thankful to the reviewers and editor for their valuable comments and suggestions made during the revision process, which greatly improved the quality of the manuscript. The first author would like to thank Gulinatti Francesca and Martinelli Ilde for their useful help on proofreading the problem of language during their visit in Beijing.

References

[1] H.S. Tsien, Superaerodynamics, mechanics of rarefied gases, J. Aeronaut. Sci. 13 (12) (1946) 653–664.
[2] G.A. Bird, Molecular Gas Dynamics and the Direct Simulation of Gas Flows, Clarendon Press, Oxford, 1994.
[3] G. Koppenwallner, H. Legge, Drag of bodies in rarefied hypersonic flow, AIAA paper 85-0998, in: J.N. Moss, C.D. Scott (Eds.), Progress in Astronautics and Aeronautics: Thermophysical Aspects of Re-entry Flows, vol. 103, American Institute of Aeronautics and Astronautics, New York, 1985, pp. 44–59.
[4] M.C. Celenligil, J.N. Moss, R.C. Blanchard, Three-dimensional rarefied flow simulations for the aeroassist flight experiment vehicle, AIAA J. 29 (1) (1991) 52–57.
[5] M.S. Ivanov, S.F. Gimelshein, Computational hypersonic rarefied flows, Annu. Rev. Fluid Mech. 30 (1998) 469–505.
[6] F. Sharipov, Hypersonic flow of rarefied gas near the Brazilian satellite during its re-entry into atmosphere, Brazilian Journal of Physics 33 (2) (2003) 398–405.
[7] S. Chapmann, T.G. Cowling, The Mathematical Theory of Non-Uniform Gases, third ed., Cambridge University Press, 1970.
[8] C. Cercignani, Kinetic Theories and the Boltzmann Equation, Lecture Notes in Mathematics, Springer-Verlag, Berlin, 1984.
[9] F.G. Tcheremissine, Advancement of the method of direct numerical solving of the Boltzmann equation, in: E.P. Muntz, D.H. Campbell (Eds.), Rarefied Gas Dynamics: Theoretical and Computational Techniques, vol. 118, AIAA, 1989, pp. 343–358.
[10] F. Roger, J. Schneider, Deterministic method for solving the Boltzmann equation, in: B. Shizgal, D.P. Weaver (Eds.), Rarefied Gas Dynamics: Theory and Simulations, vol. 159, AIAA, 1994, pp. 335–343.
[11] Z. Tan, P. Varghese, The Δ-ε method for the Boltzmann equation, J. Comput. Phys. 110 (1994) 327–340.
[12] V.V. Aristov, Direct methods for solving the Boltzmann equation and study of nonequilibrium flows, Fluid Mechanics and its Applications, vol. 60, Kluwer Academic Publishers, 2001.
[13] P.L. Bhatnagar, E.P. Gross, M. Krook, A model for collision processes in gases. I. Small amplitude processes in charged and neutral one-component systems, Phys. Rev. 94 (1954) 511–525.
[14] P. Welander, On the temperature jump in a rarefied gas, Ark. Fys. 7 (1954) 507.
[15] M.N. Kogan, On the equations of motion of a rarefied gas, Appl. Math. Mech. 22 (1958) 597.

[16] L.H. Holway Jr., New statistical models for kinetic theory, Methods Constr. Phys. Fluids 9 (9) (1966) 1658–1673.
[17] C. Cercignani, G. Tironi, Nonlinear heat transfer between two parallel plates at large temperature ratios, in: C.L. Brundin (Ed.), Rarefied Gas Dynamics, vol. 1, Academic Press, New York, 1967, pp. 441–453.
[18] P. Andries, P. Le Tallec, J. Perlat, B. Perthame, The Gaussian–BGK model of Boltzmann equation with small Prandtl number, Eur. J. Mech.: B Fluids 19 (6) (2000) 813.
[19] E.M. Shakhov, Generalization of the Krook kinetic relaxation equation, Fluid Dynamics 3 (1) (1968) 158–161.
[20] B.M. Segal, J.H. Ferziger, Shock–waves structure using nonlinear model Boltzmann equations, Phys. Fluids 15 (1972) 1233.
[21] T. Abe, H. Oguchi, A hierarchy kinetic model and its applications, in: J.I. Potter (Ed.), Progress in Astronautics and Aeronautics, vol. 51, AIAA, New York, 1977, pp. 781–793.
[22] R.D. Reitz, One-dimensional compressible gas dynamics calculations using the Boltzmann equation, J. Comput. Phys. 42 (1981) 108–123.
[23] J.M. Moschetta, D. Pullin, A robust low diffusive kinetic scheme for the Navier–Stokes/Euler equations, J. Comput. Phys. 133 (1997) 193–204.
[24] K.H. Prendergast, K. Xu, Numerical hydrodynamics from gas-kinetic theory, J. Comput. Phys. 109 (1993) 53–64.
[25] M.N. Macrossan, R.I. Oliver, A kinetic theory solution method for the Navier–Stokes equations, Int. J. Numer. Meth. Fluids 17 (1993) 177.
[26] K. Xu, Gas-Kinetic Schemes for Unsteady Compressible Flow Simulations, Twenty-ninth CFD Lecture Series 1998–2003, Von Karman Institute for Fluid Dynamics, Lecture Series, Belgium, February 23–27, 1998.
[27] C. Kim, A. Jameson, A robust and accurate LED–BGK solver on unstructured adaptive meshes, J. Comput. Phys. 143 (2) (1998) 598.
[28] K. Xu, A gas-kinetic BGK schemes for the Navier–Stokes equations and its connection with artificial dissipation and Godunov method, J. Comput. Phys. 171 (2001) 289–335.
[29] K. Xu, Z.H. Li, Microchannel flow in the slip regime: gas-kinetic BGK–Burnett solutions, J. Fluid Mech. 513 (2004) 87–110.
[30] T. Ohwada, K. Xu, The kinetic scheme for the full-Burnett equations, J. Comput. Phys. 201 (2004) 315–332.
[31] K. Xu, M. Mao, L. Tang, A multidimensional gas-kinetic BGK schemes for hypersonic viscous flow, J. Comput. Phys. 203 (2005) 405–421.
[32] Q.B. Li, S. Fu, On the multidimensional gas-kinetic BGK scheme, J. Comput. Phys. 220 (2006) 532–548.
[33] G. May, B. Srinivasan, A. Jameson, An improved gas-kinetic BGK finite-volume method for three-dimensional transonic flow, J. Comput. Phys. 220 (2007) 856–878.
[34] C.K. Chu, Kinetic-theoretic description of the formation of a shock wave, Phys. Fluids 8 (1) (1965) 12–22.
[35] E.M. Shakhov, Kinetic model equations and numerical results, in: H. Oguchi (Ed.), Proceedings of 14th International Symposium on Rarefied Gas Dynamics, vol. 1, University of Tokyo Press, Tokyo, 1984, pp. 137–148.
[36] K. Morinishi, H. Oguchi, A computational method and its application to analyses of rarefied gas flows, in: H. Oguchi (Ed.), Proceedings of 14th International Symposium on Rarefied Gas Dynamics, vol. 1, University of Tokyo Press, Tokyo, 1984, pp. 149–158.
[37] J.Y. Yang, J.C. Huang, Rarefied flow computations using nonlinear model Boltzmann equations, J. Comput. Phys. 120 (1995) 323–339.
[38] K. Aoki, K. Kanba, S. Takata, Numerical analysis of a supersonic rarefied gas flow past a flat plate, Phys. Fluids 9 (4) (1997) 1144–1161.
[39] V.A. Titarev, E.M. Shakhov, Heat transfer and evaporation from a plane surface into a half-space upon a sudden increase in body temperature, Fluid Dynamics 37 (1) (2002) 126–137.
[40] L. Mieussens, Discrete-velocity models and numerical schemes for the Boltzmann–BGK equation in plane and axisymmetric geometries, J. Comput. Phys. 162 (2) (2000) 429–466.
[41] P. Le Tallec, F. Mallinger, Coupling Boltzmann and Navier–Stokes equations by half fluxes, J. Comput. Phys. 136 (1) (1997) 51–67.
[42] N. Crouseilles, P. Degond, M. Lemou, A hybrid kinetic/fluid model for solving the gas dynamics Boltzmann–BGK equation, J. Comput. Phys. 199 (2004) 776–808.
[43] T.E. Schwartzentruber, L.C. Scallabrin, I.D. Boyd, A modular particle-continuum numerical method for hypersonic non-equilibrium gas flows, J. Comput. Phys. 225 (2007) 1159–1174.
[44] V.I. Kolobov, R.R. Arslanbekov, V.V. Aristov, A.A. Frolova, S.A. Zabelok, Unified solver for rarefied and continuum flows with adaptive mesh and algorithm refinement, J. Comput. Phys. 223 (2007) 589–608.
[45] Z.H. Li, H.X. Zhang, Numerical investigation from rarefied flow to continuum by solving the Boltzmann model equation, Int. J. Numer. Meth. Fluids 42 (2003) 361–382.
[46] Z.H. Li, H.X. Zhang, Study on gas kinetic unified algorithm for flows from rarefied transition to continuum, J. Comput. Phys. 193 (2) (2004) 708–738.
[47] D.C. Park, The Kinetic Theory of Gases with Applications in Rarefied Gas Dynamics, University of Strathclyde, Scotland, 1981.
[48] Z.H. Li, Applications of Gas Kinetic Unified Algorithm for Flows from Rarefied Transition to Continuum, Post-doctor Dissertation, Tsinghua University, Beijing, 2003.
[49] A.B. Huang, D.P. Giddens, The discrete ordinate method for the linearized boundary value problems in kinetic theory of gases, in: C.L. Brundin (Ed.), Proceedings of 5th International Symposium on Rarefied Gas Dynamics, vol. 1, New York, 1967, pp. 481–486.
[50] H.X. Zhang, F.G. Zhuang, NND schemes and their application to numerical simulation of two- and three-dimensional flows, Advances in Applied Mechanics 29 (1992) 193–256.
[51] Z.H. Li, Y.R. Xie, Technique of molecular indexing applied to the direct simulation Monte Carlo method, in: C. Shen (Ed.), Proceedings of 20th International Symposium on Rarefied Gas Dynamics, Peking University Press, Beijing, 1996, pp. 205–209.
[52] C. Cercignani, The Mathematical Theory of Dilute Gases, Springer-Verlag, New York, 1994.
[53] S. Nocilla, On the interaction between stream and body in free-molecule flow, in: L. Talbot (Ed.), Rarefied Gas Dynamics, vol. 169, Academic Press, New York, 1961.
[54] C. Cercignani, M. Lampis, Kinetic models for gas-surface interactions, Transport Theory Stat. Phys. 1 (1971) 101–114.
[55] I. Kuščer, J. Možina, F. Krizanic, The Knudsen model of thermal accommodation, in: Dini et al. (Eds.), Rarefied Gas Dynamics, vol. 1, Editrice Tecnico-Scientifica, Pisa, 1974, pp. 97–108.
[56] H. Grad, On the kinetic theory of rarefied gases, Commun. Pure Appl. Math. 2 (1949) 331–407.
[57] C. Ringhofer, C. Schmeiser, A. Zwirchmayr, Moment methods for the semiconductor Boltzmann equation on bounded position domains, SIAM J. Numer. Anal. 39 (3) (2001) 1078–1095.
[58] M.K. Gobbert, S.G. Webster, T.S. Cale, A Galerkin method for the simulation of the transient 2-D/2-D and 3-D/3-D linear Boltzmann equation, Journal of Scientific Computing 30 (2) (2007) 237–273.
[59] B. Shizgal, A Gaussian quadrature procedure for use in the solution of the Boltzmann equation and related problems, J. Comput. Phys. 41 (1981) 309–328.
[60] P. Henrici, The quotient-difference algorithm, Nat. Bur. Stand. Appl. Math. Ser. 49 (1958) 23–46.
[61] G.H. Golub, J. Welsch, Calculation of Gauss Quadrature Rules, Technical Report No. CS81, Computer Science Department, Stanford University, 1981.
[62] Z. Kopal, Numerical Analysis, Chapman and Hull Ltd., London, 1955.
[63] P.W. Peter, A. Harry, Wind tunnel measurements of sphere drag at supersonic speeds and low Reynolds, J. Fluid Mech. 10 (1962) 550–560.
[64] F.W. Vogenitz, G.A. Bird, J.E. Broadwell, H. Rungaldier, Theoretical and experimental study of rarefied supersonic flows about several simple shapes, AIAA J. 6 (12) (1968) 2388–2394.
[65] J.W. Dai, Y.G. Yang, X.G. Li, Investigation of Rarefied Gas Aerodynamics of Spacecraft Shape in Low Density Wind Tunnel, Technical Report No. S423.15, Hypervelocity Aerodynamics Institute, China Aerodynamic Research and Development Centre, 2004.